

Experimental modeling of calcium carbonate precipitation by cyanobacterium *Gloeocapsa* sp.



Irina A. Bundeleva^a, Liudmila S. Shirokova^{b,c}, Oleg S. Pokrovsky^{b,d,*}, Pascale Bénézech^b, Bénédicte Ménez^e, Emmanuelle Gérard^e, Stéphanie Balor^f

^a Université de Bourgogne, UFR Sciences de la Vie, de la Terre et de l'Environnement (SVTE), CNRS UMR 6282, 6, bd Gabriel, 21000 Dijon, France

^b Géosciences Environnement Toulouse (GET), University of Toulouse, UMR 5563 CNRS, 14 Avenue Edouard Belin, 31400 Toulouse, France

^c Institute of Ecological Problems of the North, UroRAS, 29 Naberezhnaja Sev. Dviny, Arkhangelsk, Russia

^d BIO-GEO-CLIM Laboratory, Tomsk State University, Tomsk, Russia

^e Institut de Physique du Globe de Paris—Sorbonne Paris Cité, Université Paris Diderot, CNRS UMR 7154, 1 rue Jussieu, 75238 Paris, France

^f Plateau de Microscopie électronique, FRBT CNRS FR3451, Bat. IBCG, 118 route de Narbonne, F-31062 Toulouse, France

ARTICLE INFO

Article history:

Received 28 August 2013

Received in revised form 7 March 2014

Accepted 8 March 2014

Available online 18 March 2014

Editor: Michael E. Böttcher

Keywords:

Calcite

Kinetics

Adsorption

Photosynthesis

Confocal microscopy

Raman spectroscopy

ABSTRACT

The impact of cyanobacteria *Gloeocapsa* sp. on calcium carbonate precipitation has been examined by combining physico-chemical macroscopic and *in-situ* microscopic techniques. For this, Ca adsorption and assimilation and kinetic experiments were used to assess the existence of the metabolic process responsible for CaCO₃ mineralization by *Gloeocapsa* sp. Experimental products were characterized by Scanning and Transmission Electron Microscopy (SEM and TEM) imaging, XRD analyses, coupled with Confocal Laser Scanning Microscopy (CLSM) and Raman micro-spectroscopy. Ca carbonate precipitation experiments were performed at an initial pH of 7.8 to 9.4 and 25 °C in supersaturated solutions ($\Omega_{\text{calcite}} = 1.5$ to 150) in the presence of active cyanobacterial cells. During cyanobacterial photosynthesis, the solution pH increased up to 9.5–10.8 after the first 5–10 days of growth, the Ca concentration decreased and the supersaturation index attained a maximum followed by a gradual decrease due to progressive CaCO₃ precipitation. Ca adsorption at the surface of live and inactivated *Gloeocapsa* sp. cells and Ca intracellular assimilation during cell growth were measured as a function of pH and Ca concentration in solution. The contribution of surface adsorption and intracellular uptake to total Ca removal from solution due to biocalcification does not exceed 10%. The presence of calcium carbonate, identified as calcite using Raman spectroscopy, on active *Gloeocapsa* sp. surfaces and in the vicinity of bacterial cell surfaces was evidenced using SEM. TEM and CLSM demonstrated cyanobacterial cell encrustation by CaCO₃ precipitated in the form of nano-spheres adjacent to the cell surface. In contrast to other previously investigated calcifying bacteria, no cellular protection mechanism against Ca²⁺ adsorption and subsequent carbonate precipitation has been demonstrated for *Gloeocapsa* sp. This is most likely linked to the specific cellular organization of this species, which involves several cells in one single capsule. As such, planktonic cultures of *Gloeocapsa* sp. exhibit significant calcifying potential, making them important CO₂-fixing microorganisms for both paleo-environmental reconstructions and technological applications.

© 2014 Elsevier B.V. All rights reserved.

1. Introduction

Geochemical modeling and laboratory experiments have demonstrated the importance of both physico-chemical mineral nucleation/precipitation processes and specific metabolic reactions in the overall microbially-induced CaCO₃ biomineralization processes that have occurred for most of Earth's history (Merz, 1992 and references therein). Various carbonate biomineralization mechanisms based on cyanobacteria cellular metabolism and surface composition have been proposed (Merz

et al., 1993; McConnaughey and Whelan, 1997; Dittrich and Obst, 2004; Martinez et al., 2008; Obst et al., 2009a, b; Couradeau et al., 2012). Arp et al. (2001) discussed, using a modeling approach, the various parameters needed for cyanobacteria encrustation and concluded "that Phanerozoic oceans sustaining calcified cyanobacteria must have had considerably higher calcium concentrations than oceans of today." As such, it was suggested that the lack of calcified cyanobacteria in stromatolite-bearing Precambrian sequences could be due to high dissolved inorganic carbon concentrations (Arp et al., 2001). However, systematic experimental studies of CaCO₃ biomineralization by cyanobacteria at highly variable calcium to total inorganic carbon ratios in a wide range of supersaturation state are very limited (e.g., Obst et al., 2009b).

* Corresponding author at: Université de Bourgogne, UFR Sciences de la Vie, de la Terre et de l'Environnement (SVTE), CNRS UMR 6282, 6, bd Gabriel, 21000 Dijon, France.
E-mail address: oleg@get.obs-mip.fr (O.S. Pokrovsky).

Cyanobacteria have been clearly associated with freshwater calcium carbonate biomineralization. Some attribute this link to Ca^{2+} binding to cyanobacteria surfaces (Thompson and Ferris, 1990; Castanier et al., 1999; Dittrich and Sibling, 2005, 2006; Liang et al., 2013). It has also been postulated that cyanobacterial calcification results from the rise of pH at the cell surface stemming from bicarbonate/nutrient assimilation (Merz, 1992; McConnaughey and Whelan, 1997). However, other studies have concluded that calcium carbonate nucleation is initiated on inert bacteriogenic organic nano-globules and exopolymeric substances (Aloisi et al., 2006), and precipitation of amorphous CaCO_3 within the extracellular polymers of cyanobacteria could serve as a protection mechanism against uncontrolled precipitation of calcite at their surface (Obst et al., 2009a). Indeed, the microbial cell surface and excreted extracellular polymeric substances (EPS), which carry a net negative electric charge and have the capacity to bind Ca^{2+} ions, are frequently considered as sites of carbonate nucleation (Dupraz et al., 2004; Braissant et al., 2007; Obst et al., 2009c; Paulo and Dittrich, 2013a). The role of photosynthesizing cyanobacteria on carbonate mineralization under cell entombment conditions is, however, paradoxical, which has been noted only recently (Martinez et al., 2010). To successfully photosynthesize, these bacteria must acquire aqueous bicarbonate ions or aqueous CO_2 (Price et al., 2002). Bicarbonate ion consumption generates hydroxide ions, increasing pH and thus inducing calcite supersaturation and precipitation, which leads to cell encrusting and entombment (e.g., Thompson and Ferris, 1990; Merz, 1992; Verrecchia et al., 1995; Sanchez-Roman et al., 2008; Jiang et al., 2013; Liang et al., 2013; Paulo and Dittrich, 2013b). Therefore, different cyanobacteria (Martinez et al., 2010) as well as heterotrophic aerobic and anaerobic bacteria (Aloisi et al., 2006; Bontognali et al., 2008) possess a self-protection mechanism against uncontrolled CaCO_3 coating and live cell embedding. For *Synechococcus*, *Planctothrix* and anoxygenic phototrophic bacteria (APB), this protection mechanism consists of maintaining a positive surface potential in alkaline solutions, avoiding Ca adsorption at the cell surface (Martinez et al., 2008, 2010; Bundeleva et al., 2011, 2012). The surface potential regulation occurs via multiple and still poorly identified molecular and physiological mechanisms occurring in the vicinity of cell membrane. Examples of such mechanisms could be: conformational changes in the S-layer protein arrangement (Rachel et al., 1997), lysine-rich protein production within the cytoplasmic membrane (Zinovieva et al., 1998), proton secretion by the APB cell wall via proton-pumping (McConnaughey and Whelan, 1997) and enhanced respiration under alkaline conditions required to keep the proton gradient stable (Bazant et al., 2009).

The highly versatile cyanobacterium, *Gloeocapsa* sp., occurring in freshwater to hypersaline environments, is different from other unicellular microorganisms studied thus far in the sense that it possesses a thick spherical polysaccharidic capsule surrounding several cells attached together. The presence of this capsule increases the distance between the cell surface membrane and the external environment. As a result, though the individual cells of *Gloeocapsa* may be able to protect themselves via some electrostatic mechanism, this protection could fail within the cell aggregates, when the cell membrane and external solution are separated by the rigid capsule. In other words, because of the significant distance between the cell membrane and aqueous solution, the metabolically induced electrostatic potential cannot control the Ca/bicarbonate approach to the surface of the capsule and thus cannot regulate the protective response. In this case, live *Gloeocapsa* cells may turn out to be extremely efficient calcifiers that are capable of extensive CaCO_3 precipitation in the vicinity of the cells directly during their life cycle, without necessary participation of dead cells or heterotrophic bacteria as is known for other calcifying cultures. Therefore, it can be hypothesized that cyanobacterium *Gloeocapsa* has not any protection mechanism against the carbonate encrustation and these bacteria can be the effective carbonate producer in various Earth surface environments.

The present work is aimed at verifying this hypothesis by assessing the rates and mineralogical nature of CaCO_3 precipitation during

Gloeocapsa photosynthesis over a very large range of solution supersaturation and Ca/(Dissolved Inorganic Carbon) ratios. For this, carbonate precipitation experiments have been conducted in closed-system reactors in the presence of active *Gloeocapsa* sp. under light and dark conditions. Solid precipitates and cell surfaces were characterized using scanning and transmission electron microscopy, coupled to energy-dispersive X-ray spectroscopy (SEM- and TEM-EDX); complementary investigations were carried out using confocal laser scanning microscopy (CLSM) coupled to Raman microspectroscopy and measurements of Ca^{2+} adsorption and assimilation by live bacteria. The results reported here aim at illuminating the high capacity of selected cyanobacterium to induce carbonate precipitation during photosynthesis, which may have important implications for various biomineralization scenarios.

2. Materials and methods

2.1. *Gloeocapsa* sp. cultures

Pure culture of cyanobacteria *Gloeocapsa* sp. f-6gl was used in this study. This cyanobacterium previously described in Pokrovsky et al. (2008) is characterized by small number of cells enclosed within concentric and rigid mucilage envelopes. The individual colonies are spherical, microscopic. The purity of the culture has been regularly controlled by optical microscope examination and by cultivation on nutrient BG-11 agar. The concentration of the suspended bacterial cell was quantified by (1) measurement of the absorbance (i.e. optical density, OD) of suspensions using a spectrophotometer at a wavelength of 750 nm with a calibration curve OD as a function of humid weight that was linear up to 1.3 OD units, (2) weighing the wet centrifuged pellets (20 min at 5000 g) and (3) freeze-drying the centrifuged pellets. The ratio between the humid and freeze-dried weight of *Gloeocapsa* sp. was 10.0 ± 2.0 . The biomass quantification via the light absorbance measurement could be biased because of the presence of precipitated Ca carbonate. The 750 nm wavelength was accordingly selected after full spectra recording in the 300–800 nm region of both mineral-free live cells of *Gloeocapsa* sp. cyanobacteria and cell-free calcite suspensions. The mineral suspension did not exhibit any adsorption in the region 650–800 nm whereas the cyanobacterial cells exhibited a distinct peak at 700–750 nm. The overall light absorbance of the mineral suspension was lower by a factor of 10 than that of live biomass, when expressed per dry and wet weight. As a result, the maximum uncertainty in optical biomass measurements induced by the presence of minerals via absorbance at 750 nm was $\leq 10\%$, which is within experimental reproducibility limits.

2.2. Growth and preparation of *Gloeocapsa* sp. prior to the experiments

Gloeocapsa sp. was cultured until stationary growth phase in EDTA-free 10% Cyanobacteria BG-11 Fresh-water Solution Medium (Sigma-Aldrich C3061, Rippka et al., 1979). This culture media was specially modified from normal, nutrient-rich BG-11 solution to avoid the modification of the EPS structure and composition and other surface properties of bacteria in the laboratory compared with strongly dilute natural environments (Hunter et al., 2010). Indeed, it is known that different planktonic cyanobacterial strains are capable of altering both the amount and properties of EPS they produce depending on the nutrient concentration during cell division (Obst et al., 2009c). Compared with normal culture conditions, the stationary growth phase of *Gloeocapsa* sp. in 10-times diluted BG-11 was achieved two to three weeks after inoculation, and stationary culture was maintained for at least three weeks. Stock cultures of *Gloeocapsa* sp. were kept at 25 ± 1 °C under constant cool white fluorescent light (2000 lx) on a Ping-Pong Fisher shaker. The cultures for experiments were harvested at the beginning-to-medium stationary growth stage by centrifugation at 4000 g for 10 min at 20 °C. The cells were rinsed in 0.1 M NaCl, which corresponded to optimal physiological conditions and centrifuged

twice at 4000 g for 10 min. Finally, the bacterial suspension was washed in appropriate electrolyte solution (0.1 M NaCl) and centrifuged.

Inactivated cells were prepared by rinsing part of the fresh (live) biomass in 0.01 M sodium azide (NaN_3) for 1–2 h. Sodium azide suppresses bacterial activity by inhibiting cytochrome oxidase and is widely used for inactivating cells while keeping the surfaces physically and chemically intact (Hunter et al., 2010). The cell growth of *Gloeocapsa* sp. culture in the presence of 0.01 M NaN_3 in nutrient solution was completely suppressed as proven in a separate series of experiments.

2.3. Experimental procedure and analyses

2.3.1. Ca adsorption on cell surfaces

In this study, two aspects of the Ca^{2+} adsorption process were characterized: i) adsorption at constant initial calcium concentration in solution as a function of pH (pH-dependent adsorption edge) and ii) adsorption at constant pH as a function of calcium concentration in solution (adsorption isotherm). All experiments were performed in solutions undersaturated with respect to any calcium carbonate phase as verified by speciation calculations using the MINTEQA2 program and corresponding database (Allison et al., 1990).

In experiments with *Gloeocapsa* sp., the initial calcium concentration at variable pH ranged between 2.3 and 17 μM , whereas the Ca concentration in constant-pH experiments was between 4.2 and 25 μM (Table 1). The background electrolyte used for these experiments was always 0.1 M NaCl. The pH was adjusted by adding aliquots of NaOH (0.1 and 0.01 M) or HCl (1.0, 0.1 and 0.01 M), whereas the constant pH of 7.6, 9.0 and 11.8 was maintained by adding 5 mM HEPES (4-(2-hydroxyethyl)-1-piperazineethanesulfonic acid), 5 mM NaHCO_3 + Na_2CO_3 and 5 mM Na_2CO_3 buffers, respectively.

The effect of light on Ca^{2+} adsorption onto the surface of *Gloeocapsa* sp. was also investigated. For this, adsorption experiments were run under light (2000 lx) or in the darkness, by wrapping the vials with aluminum foil. Adsorption experiments were conducted in 8 mL sterile polypropylene vials for 2.5, 19 and 24 ± 1 h at 25 ± 0.2 °C in continuously agitated bacteria suspension with an ionic strength of 0.1 M NaCl. The biomass concentration was kept constant at 10 $\text{g}_{\text{wet}}/\text{L}$. Live, freshly harvested (stationary stage) cells, sodium azide-inactivated and heat-killed (autoclaved 20 min at 120 °C) bacteria were used in the adsorption experiments. The cells were rinsed in 0.1 M NaCl and 0.01 M EDTA solutions for 12 min and again in 0.1 M NaCl solution prior the experiments. This procedure allowed desorption of all possible Mg^{2+} and Ca^{2+} ions from the cell surfaces that might have occurred during the cyanobacteria culturing. The removal of EPS during rinsing and EDTA treatment was tested via analysis of dissolved organic carbon (DOC) of 0.45 μm -filtered solution after each step of rinsing. We found an insignificant increase of the DOC in the supernatant solution after rinsing in a total amount of less than 1% of the biomass.

The adsorption of calcium on cell surfaces was quantified by subtracting, at each solution pH, the concentration of calcium remaining

in the bacterial suspension from the concentration of calcium added in the supernatant. The adsorption of calcium on reactor walls, Ca precipitation as insoluble Ca carbonate, and cellular Ca release from the biomass in the full range of studied pH was negligible (<10%) compared with the initial amount of Ca added. This was routinely verified by Ca analyses in the supernatant and in the zero-added-Ca cell suspension experiments. The measured Ca concentrations in these experiments, often at the limit of analytical detection, were explicitly taken into account to calculate the adsorption isotherm. Additional blank adsorption experiments were performed in the same vials and initial Ca concentration without addition of cells, using cell supernatant in the background electrolyte as adsorption medium. The adsorption of Ca on reaction cell walls and filter material did not exceed 10% of that adsorbed on cells and was also taken into account when calculating the adsorption yield. The DOC concentration during adsorption measurements remained constant, between 5 and 10 mg/L and did not vary with pH and ionic strength in any systematic manner, suggesting negligible cell lysis and degradation in the full range of studied solution conditions.

2.3.2. Ca uptake during cell growth

There are three possible sinks for Ca in bacterial suspension: (1) metabolic intracellular incorporation during growth, (2) reversible adsorption at the cell surface and adjacent EPS and (3) calcium precipitation in the form of CaCO_3 . To characterize the Ca metabolic uptake by live cyanobacteria, Ca concentration evolution was followed in the experiments with bicarbonate-free nutrient solution, containing 0.5 and 5 mM Ca, where CaCO_3 precipitation did not occur ($\Omega_{\text{calcite}} \leq 0.5$). Experiments were performed in glass bottles closed by wadded stopper shaken under light at 25 ± 1 °C. Periodically, aliquots of homogeneous suspension were sampled and used for measurements of biomass, pH and, in <0.22 μm filtered samples, of Ca and alkalinity. Regular optical examination of cyanobacterial cells demonstrated that they remained intact, preserving their envelopes and structural organization in 2–4 cell associates within a single capsule.

2.3.3. Mineral precipitation experiments

Kinetic experiments were performed in nutrient phosphate-free solution (10% BG-11 medium without phosphate) and in inert electrolyte solution (0.1 M NaCl) at 25 ± 1 °C in stirred Schott® 1 L glass bottle reactors containing 800 mL of the fluid. The bottles were closed by sterile ventilated caps (Biosilico®) allowing efficient gas exchange with the atmosphere and were kept at 25 ± 1 °C and continuously illuminated (white light at 2000 lx) in respect the light/dark cycle 12 h/12 h. Preliminary experiments in 10% BG-11 containing normal phosphate concentration and enriched in Ca and bicarbonate yielded Ca phosphate as a mineral precipitate induced during cell photosynthesis. Additionally, phosphate from the nutrient media is known to produce various artifacts during carbonate mineralization experiments (Gallagher et al., 2013). To avoid phosphate mineral precipitation and a phosphate effect

Table 1
Summary of Ca adsorption with *Gloeocapsa* sp.

No.	Durations, h	Biomass, mg wet/L	Conditions	[Ca] range, μM	pH range
<i>pH edge adsorption</i>					
1	2.5	10	0.1 M NaNO_3	2.28–19.1	2.981–11.429
2	2.5	10	0.1 M NaCl	3.30–70.1	2.537–8.011
3	24	10	0.1 M NaCl	12.6–81.2	2.564–11.206
4	24	10	0.1 M NaCl	17.0–65.4	2.578–11.588
<i>Langmuirian adsorption</i>					
5	24	20	0.1 NaCl	24.5–50.0	7.74–7.89
6	19	10	6 ml 0.1 M NaCl + 0.3 ml 0.1 M NaHCO_3	13.6–69.1	11.80–11.82
7	24	10	6 ml 0.1 M NaCl + 0.3 ml 0.1 M HEPES	13.7–93.6	7.60–7.62
8	24	10	6 ml 0.1 M NaCl + 0.3 ml 0.1 M HEPES	4.20–75.7	8.99–9.10
9	24	10	6 ml 0.1 M NaCl + 0.3 ml 0.1 M HEPES	5.25–718	7.51–7.48
10	23	10	6 ml 0.1 M NaCl + 0.3 ml 0.1 M HEPES	6.80–727	6.95–7.56

Table 2

Kinetic experiments with *Gloeocapsa* sp.: conditions, rates and mineralogy of precipitates.

No.	Duration, h	Biomass range, g _{wet} /L	pH range	[Alkalinity] range mM	[Ca] range mM	Precipitation rate (R), μM/h	Ω range	[DOC], mM	Mineralogy (XRD)
<i>Biotic experiments in nutriment solution</i>									
1 ^a	1296	0.22–0.36	7.85–8.09	1.14–1.11	1.97–1.81	0	1.58–3.47	NM	ND
2	1296	0.24–0.46	7.84–7.95	1.63–1.20	1.85–1.40	5.83	2.09–3.02	NM	Calcite
3 ^a	456	1.21–1.98	8.17–8.82	1.14–0.83	2.70–2.07	0.00	4.07–8.91	NM	ND
4	456	0.88–1.85	8.12–8.94	1.62–0.75	2.54–1.41	4.73	4.09–7.58	NM	Calcite
5	1296	0.26–0.28	7.94–8.19	3.83–2.28	1.73–0.70	10.4	6.37–2.57	NM	Calcite
6 ^a	1032	0.91–2.00	7.88–8.20	1.69–0.70	6.30–4.62	19.7	6.03–4.07	NM	Calcite
7 ^a	1032	1.04–2.59	8.08–8.20	1.07–0.55	6.81–5.04	3.09	6.31–3.39	NM	Calcite
8	456	0.90–2.02	7.92–8.28	2.02–0.80	6.23–4.50	15.2	7.94–5.37	NM	Calcite
9	408	0.12–2.92	8.58–9.82	0.70–1.47	13.1–10.8	15.8	15.1–79.4	NM	ND
10	1824	0.54–0.69	8.08–7.87	3.90–1.42	5.04–3.15	5.03	17.8–3.02	NM	Calcite
11	1824	0.53–0.29	7.84–7.97	8.33–7.21	0.94–0.20	0.86	19.1–5.13	NM	Calcite
12	3275	0.17–1.08	8.64–9.76	4.43–2.32	1.52–0.09	2.92	23.1–6.64	0.81–2.96	Calcite
13	1032	0.94–2.76	8.11–9.33	4.28–0.94	6.19–2.41	17.8	4.28–0.94	NM	Calcite
14	3275	0.17–1.02	8.66–9.75	17.5–6.63	0.77–0.07	6.48	24.5–8.30	0.66	calcite
15	120	0.15–0.84	7.46–8.34	10.0–0.59	20.0–10.9	76.1	29.5–7.80	NM	Calcite + aragonite
16	408	0.14–2.7	8.69–9.10	1.43–1.89	9.19–7.46	19.2	30.9–61.6	NM	ND
17	120	0.15–1.48	7.75–8.58	10.0–0.97	10.0–1.80	68.3	34.7–43.7	NM	Calcite
18 ^a	120	0.04–0.74	8.86–9.99	4.27–2.80	1.80–0.09	14.2	38.1–6.30	NM	ND
19	552	0.19–0.45	8.62–9.02	4.36–3.12	1.48–0.31	2.12	42.6–5.30	NM	ND
20	356	0.10–1.52	7.71–8.54	10.0–0.31	20.0–9.26	53.5	50.1–8.10	NM	Calcite
21	408	0.12–1.98	8.27–9.56	2.61–0.94	45.0–38.2	54.2	57.7–53.7	NM	ND
22	408	0.18–1.92	9.00–9.07	4.56–2.66	2.75–1.47	6.48	69.2–30.9	NM	ND
23	264	0.68–1.22	9.10–8.71	2.44–2.98	5.80–7.73	0	70.8–58.9	NM	ND
<i>Biotic experiments in nutrient solution</i>									
24	120	0.04–0.60	8.82–10.81	4.30–0.88	4.50–0.45	56.2	70.8–6.30	NM	ND
25 ^a	356	0.15–1.22	9.37–9.49	10.0–7.95	1.00–0.09	2.57	75.8–6.70	NM	ND
26	264	0.15–1.88	9.37–9.73	10.0–4.40	1.00–0.87	7.64	75.9–8.90	NM	ND
27	408	0.12–2.76	8.44–9.45	3.75–1.03	20.6–18.8	25.0	74.9–54.9	NM	ND
28	408	0.14–2.62	8.83–9.46	4.53–1.49	4.83–3.47	9.12	79.4–50.1	NM	ND
29	168	0.15–0.9	8.17–9.51	10.0–0.50	10.0–2.13	65.6	81.3–13.8	NM	Calcite
30	264	0.62–1.46	9.56–9.01	2.84–3.36	2.77–2.74	3.06	89.1–54.9	NM	ND
31	264	0.15–3.16	8.51–9.10	10.0–4.85	5.00–0.46	21.2	93.3–18.2	NM	ND
32	284	0.04–2.28	8.73–8.62	4.96–0.77	9.00–2.69	135	107–12.3	NM	Calcite
33	216	0.15–1.62	8.79–9.49	10.0–2.53	5.00–0.22	22.1	147–9.80	NM	ND
<i>Biotic experiments in inert electrolyte</i>									
34 ^a	94	1.66–2.00	8.96–10.9	4.95–2.93	3.45–2.59	9.68	66.1–117	NM	ND
35	94	1.64–1.96	9.07–10.8	4.42–3.98	3.40–3.05	1.82	83.2–186	NM	ND
36	94	1.50–1.80	8.84–10.7	4.62–2.08	6.52–5.49	12.0	85.1–114	NM	ND
37	94	1.60–1.74	8.90–10.6	4.18–2.40	5.11–3.94	40.5	93.3–107	NM	ND
<i>Biotic experiments in nutriment solution without light</i>									
38	3275	0.08–0.17	8.37–9.17	4.91–2.68	1.52–0.12	2.44	23.4–3.90	0.17–0.44	ND
39	3275	0.08–0.18	8.66–9.69	6.99–13.34	0.77–0.08	0.05	24.5–6.80	0.21	ND
<i>Abiotic experiments (with autoclaved bacteria) in nutriment solution</i>									
40	456	Bacteria free	7.54–7.42	1.42–1.21	5.00–6.40	0.00	2.57–1.62	NM	NP
41	456	Bacteria free	7.90–8.18	4.45–4.20	6.25–5.94	0.00	16.2–22.4	NM	NP
42	456	Bacteria free	8.28–8.22	4.90–4.40	2.30–2.15	0.00	17.8–13.5	NM	NP
<i>Blank (without bacteria) experiments in nutriment solution</i>									
43 ^a	120	Bacteria free	7.40–8.01	10.0–0.83	20.0–7.96	100	25.7–4.70	NM	Calcite
44	356	Bacteria free	7.42–7.89	10.0–0.81	20.0–9.04	30.8	26.9–4.70	NM	ND
45	284	Bacteria free	8.60–7.89	4.47–0.80	9.00–5.45	12.5	79.4–2.70	NM	ND
<i>Ca uptake during bacterial growth in nutriment solution</i>									
46 ^a	1518	0.08–1.308	9.32–10.15		0.008–0.000			NM	
47	1518	0.097–1.324	9.30–9.96		0.011–0.000			NM	
48 ^a	1518	0.074–1.159	9.15–9.82		0.53–0.42			NM	
49	1518	0.074–1.189	9.18–9.68		0.55–0.39			NM	
50 ^a	1518	0.074–1.055	8.37–8.72		5.33–4.87			NM	
51	1518	0.069–1.019	8.13–8.80		5.23–4.83			NM	

NM: not measured.

ND: not determined.

NP: not precipitated.

^a Experiments performed in duplicates.

on CaCO₃ precipitation rates, all 10% nutrient solution used for kinetic experiments did not include orthophosphate.

Kinetic experiments were conducted with the initial concentration of calcium chloride and sodium bicarbonate ranging from 1 to 50 and 5 to 10 mM, respectively. All biotic experiments were performed with

an initial biomass concentration between 0.04–0.68 g_{wet}/L (in the 10% nutrient solution) and 1.5–1.7 g_{wet}/L (in the inert electrolyte). High initial biomass concentration in inert electrolyte, where no bacterial growth occurred, was chosen in order to match the typical concentration in experiments with CaCO₃ precipitation. The variation of the

biomass during the experiments was explicitly taken into account for rate calculations. Precipitation experiments were conducted using a wide range of initial saturation index (Ω_{calcite}) values varying between 1.5 and 150 in the nutrient solution and between 60 and 90 in the inert electrolyte solution. The range of Ω_{calcite} in the nutrient solution was within the values reported for various natural settings such as (i) Lake Constance, between 1 and 10 with a maximal value of 31 (Stabel, 1986); (ii) freshwater lakes, between 1 and 4 (Dittrich and Obst, 2004); and (iii) freshwater streams, typically <10 (Merz-Preiss and Riding, 1999). The range of Ω_{calcite} in the inert electrolyte solution was also wide because the experiments with *Gloeocapsa* sp. at lower supersaturation failed to precipitate calcite. For live bacteria, we also tested very high supersaturation degrees (10 to 150) to imitate the local supersaturation raised within the biomats, where the local pH may be one to two units higher relative to the bulk solution, and Ω_{calcite} values as high as 20 to 50 are not uncommon (Bissett et al., 2008; Shiraishi, 2012 and references therein). The initial experimental conditions investigated in this study are listed in Table 2. Approximately 20% of the experiments were conducted in duplicates (see Table 2). Regardless of the degree of atmospheric CO_2 exchange with the reacted solution, CaCO_3 supersaturation indices were rigorously calculated in Ca– CO_2 – H_2O system from the pH and alkalinity measurements at each sampling point.

Regularly, an aliquot of ~7 mL was removed from the reactor, using a sterile syringe or pipette, to monitor the chemical and microbiological evolution of the system. Approximately 2 mL of this aliquot was used to estimate the concentration of bacterial cells in the reactor by measuring optical density at a 750 nm wavelength and then pH. The remaining 5 mL was filtered through a 0.22 μm filter to remove the biomass from the suspension. The filtrate was analyzed for alkalinity and calcium concentration.

The pH in each unfiltered sample was measured using a Fisher® pH combined electrode, with an uncertainty of 0.01 units, previously calibrated using pH 4.01, 6.86, 9.18 and 10.01 buffer solutions at 25 °C. All filtered (0.22 μm) solutions were analyzed for aqueous Ca concentration using flame atomic absorption spectroscopy (Perkin Elmer AAnalyst 400) with an uncertainty of $\pm 2\%$ and a detection limit of 0.5 μM . Dissolved Inorganic Carbon (DIC) was obtained from pH and alkalinity, which was determined by HCl titration using an automatic Schott TitroLine alpha TA10^{plus} titrator with an uncertainty of $\pm 2\%$ and a detection limit of 5×10^{-5} M. DOC was analyzed using a Carbon Total Analyzer (Shimadzu SCN) with an uncertainty of 3% and a detection limit of 0.05 mg/L.

The speciation and saturation state of the reactive fluids with respect to potentially precipitating mineral phases for all experiments was calculated using PHREEQC (Parkhurst and Appelo, 1999) software together with the MINTEQA database (Allison et al., 1990). These calculations were performed based on [Ca], pH and alkalinity measurements at each sampling point.

Rate and concentration data were analyzed with best fit functions based on the method of least squares, Pearson correlation and one-way ANOVA with the STATISTICA version 8 software (StatSoft Inc., Tulsa, OK). Regressions and power functions were used to examine relations between biocalcification rates and aqueous solution parameters such as pH, DIC, Ca, Ca/DIC and Ω_{calcite} . Correlation coefficients were calculated to elucidate relations between rates or amount of Ca removed from solution and solution parameters. A criterion of a significant correlation between elements was Pearson coefficients that were higher than 0.5 ($R^2 \geq 0.5$).

2.4. Solid phase analyses

2.4.1. Electron microscopy

Mixtures of *Gloeocapsa* sp. cells and precipitated mineral phase were subjected to digestion for removal of organic matter using a 2–3 day treatment in 10% H_2O_2 at the same solution pH as in experimental samples. The resulting solid phases were rinsed in MilliQ water, stored at

– 80 °C and freeze dried. Selected samples were studied using X-ray diffraction (INEL CPS 120, $\text{Co}_{\text{K}\alpha}$, scan speed 0.02 s^{-1}), and microscopic examination was performed using a JEOL JSM840a Scanning Electron Microscope (SEM) equipped with a field emission gun and a JEOL EDS detector, operating at 80 kV and 200 kV after carbon film coating on the sample surface.

Aliquots of suspensions containing untreated live bacterial cells and precipitated minerals were also examined using Transmission Electron Microscopy (TEM) with a JEOL JEM 12000 EX and a JEOL JEM 2100 F (equipped with a field emission gun and PGT EDX detector) at 80 kV. The cell suspension was rinsed using sterile nutrient solution or MilliQ water, centrifuged 2 min at 7000 g. Samples were taken by immersing grids coated with a carbon film for 10 s in prepared bacterial suspension and dried several minutes to several hours at room temperature. It is possible that the drying procedure could lead to artifactual tight association of cells and minerals together and thus interfere with our interpretation of precipitation products. We tested the effect of the duration of the drying procedure on the resulting TEM images and did not detect any significant difference in cell and mineral size, shape and the degree of their association. Images of cell-free mineral suspension and mineral-free cell suspension yielded morphologies very similar to those in the ternary (cell + mineral in solution) systems. However, the main proof of the validity of the cell preparation procedure used in this study was acquired *via* confocal laser scanning microscopy (CLSM) as described below.

2.4.2. Combined CLSM and Raman microspectroscopy

The coupling of these two techniques allowed to understand the spatial organization of bacterial cells and mineral associates with minimal interferences due to sample preparation procedure (Gérard et al., 2013; Paulo and Dittrich, 2013b; Bundeleva et al., 2014). For these characterizations, 2–3 weeks after the beginning of the experiments, an aliquot of bacterial–mineral suspension (~1 mL) was removed from the closed-system reactor using a sterile syringe or a pipette and immediately deposited on a thin CaF_2 window, previously washed with 70% ethanol. The sample was air-dried before measurements. This suspension was examined using a FluoView™ FV1000 confocal laser scanning microscope with a spectral resolution of 2 nm and a spatial resolution of 0.2 μm (Olympus) combined with an Invia Raman Spectrometer (Renishaw).

The FluoView™ FV1000 is equipped with a 405 nm laser diode, and multi-line argon (458 nm, 488 nm and 515 nm), helium-neon-green (543 nm) and helium-neon-red (633 nm) lasers (Gérard et al., 2013). An oil immersion objective UPLSAPO 60XO (Olympus; 60 \times magnification, N.A. = 1.35) was used for the freshly-collected suspension examination. Fluorescence images stacks were obtained with concomitant excitation at wavelengths of 405 nm, 515 nm and 633 nm by collecting the emitted fluorescence between 425–475 nm, 520–550 nm and 640–800 nm, respectively. Images were acquired, visualized and processed using F10-ASW FLUOVIEW software.

The Invia Raman Spectrometer (Renishaw) used the 785 nm wavelength of a laser diode source focused through the CLSM microscope with $\times 50$ and $\times 100$ objectives (numerical aperture: 0.75 and 0.9, respectively). This configuration yields a planar resolution close to 1 μm . Light was dispersed by a holographic grating with 1200 grooves/mm and the signal analyzed with a RENCAM charge-coupled device (CCD) detector. PMT and confocal imaging were used to locate the areas of interest for Raman spectra acquisition. Linescan spectra were acquired from several locations of the sample in order to ensure the representativeness of the Raman signal. Typically, 3 Raman spectra were collected during 10 s from several locations of the sample in order to ensure their representativeness. Extended mode analysis in the range of 130–4000 cm^{-1} was used to characterize the constitutive components of the experimental solid byproducts that were deposited on transparent CaF_2 windows. Raman spectra were acquired and characterized using the software Wire 3.2 (Renishaw). Identification of the carbonates

was made by comparison with the RRUFF™ database (www.ruff.com; Downs, 2006).

3. Results

3.1. Calcium adsorption

The experimental conditions in adsorption experiments are listed in Table 1. The pH-dependent adsorption edge for *Gloeocapsa* sp. in 0.1 M NaCl, $[Ca]_{initial} = 74 \mu M$ with a biomass of $10 g_{wet} L^{-1}$ exposed for 3 h in the dark is illustrated in Fig. 1. As seen from this figure, the adsorption is very low at $pH < 3$, it increases to 25–30% at $pH = 5-6$ and gradually increases to 30–35% with a further pH increase, up to 11.5. There is no significant difference in the adsorption yield for cells kept in the darkness during 3 h and those exposed to light during 24 h. The maximal concentration of adsorbed Ca^{2+} is 2 to $3 \mu mol g_{wet}^{-1}$.

Calcium adsorption isotherms recorded for live *Gloeocapsa* sp. at three constant pH values (7.6, 9.0 and 11.8) and Ca concentrations from 10 to $100 \mu M$ during 24 h under continuous illumination are illustrated in Fig. 2. The measured maximal adsorption density is close to 2 to $2.5 \mu mol g_{wet}^{-1}$, which is in accordance with results of pH-dependent adsorption edge. The trend of adsorbed concentration as a function of aqueous Ca^{2+} is rather similar for all three studied pH values. There are some 10–20% differences between the adsorption yield at different pH with the highest adsorption observed at $pH = 7.6$ without added $NaHCO_3$ followed by that at $pH 11.8$ and 9.0 in the presence of 5 mM $NaHCO_3$.

3.2. Ca and DIC uptake during bacterial growth

Ca is an essential structural and metabolic component of cyanobacterial cells where it can present in the cytoplasm, cell surface EPS or incorporated as storage compounds (Ca phosphates and oxalates).

The results for Ca uptake during cyanobacterial growth are illustrated in Fig. 3. Plotted in this figure are the biomass, pH and Ca concentration evolution in experiments that lasted 65 days. As seen, there is an increase of the biomass (up to $1.15 g_{wet} L^{-1}$) and pH (up to 11.4) during growth in the presence of various Ca concentrations. At the same time, only a small decrease of calcium concentration ($\leq 0.1-0.5$ mM) is observed, whereas the DIC concentration remains constant or slightly increased (not shown), indicating the absence of carbonate mineral precipitation. Optical microscopic examination of suspension supernatant and reactor walls did not indicate any secondary mineral presence. We believe that the observed Ca concentration decrease is due to Ca adsorption plus intracellular incorporation. The maximal amount of

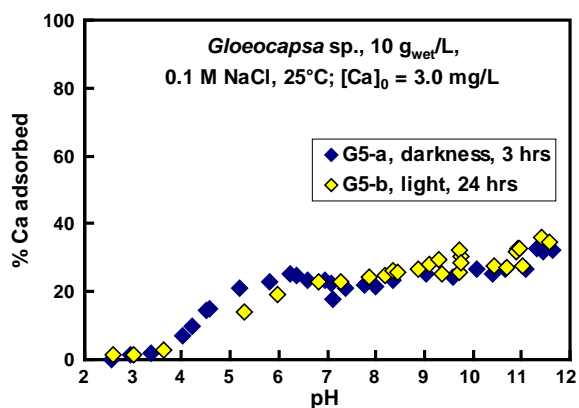


Fig. 1. Percentage of adsorbed calcium as a function of pH for live *Gloeocapsa* sp. culture in the darkness (blue diamonds) and under light (yellow diamonds). Experimental conditions: $25^\circ C$, $[Ca]_0 = 75 \mu M$, $10 g_{wet}$ biomass/L in 0.1 M NaCl and 3 to 24 h of light exposure time. The error bars are within the symbol size. (For interpretation of the references to color in this figure legend, the reader is referred to the web version of this article.)

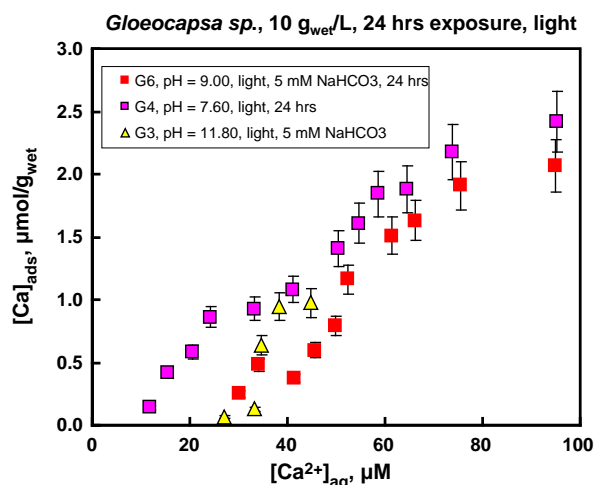


Fig. 2. Concentration of adsorbed calcium as a function of calcium concentration in solution (constant-pH adsorption isotherm) for live *Gloeocapsa* sp. Experimental conditions: $25^\circ C$, pH 7.6, 9.0 and 11.8, $10 g_{wet}$ biomass/L in 0.1 M NaCl and 24 h of light exposure.

calcium that active bacteria are capable of uptaking during their growth was calculated from the difference between the initial and final Ca concentration normalized to final cell biomass as follows:

$$[Ca]_{uptake} = ([Ca]_{initial} - [Ca]_{final}) / \text{biomass}_{final} \quad (1)$$

For *Gloeocapsa* sp., the maximal uptake of calcium in the cells in our experimental conditions ranged from 86 to $430 \mu mol Ca g_{wet}^{-1}$, which was significantly higher than the experimental adsorption site density ($\sim 2 \mu mol g_{wet}^{-1}$, see Section 3.1). At the same time, Ca incorporation in live *Gloeocapsa* cells is much higher than that in anoxygenic phototrophic bacteria (13 to $8 \mu mol Ca g_{wet}^{-1}$; Bundeleva et al., 2011). Taken together, the maximal metabolic and passive adsorptive Ca uptaken by live *Gloeocapsa* sp. not linked to carbonate mineral precipitation is $430 \mu mol Ca g_{wet}^{-1}$.

3.3. Kinetic of $CaCO_3$ precipitation in the presents of *Gloeocapsa* sp.

Temporal variation of all experimental parameters in each individual experiment is presented in the electronic supplementary material (Table ESM), whereas the initial conditions of the conducted experiments are listed in Table 2. The number of individual experiments in Table 2 corresponds to those in the Table ESM.

Three types of biotic kinetic experiments were conducted (Table 2): live culture in phosphate-free 10% nutrient solution (Table A of the ESM), in the inert electrolyte 0.1 M NaCl (Table B of the ESM) and live culture without light in phosphate-free nutrient solution (Table C of the ESM). In most experiments conducted in this work, the precipitation process can be broken down into three stages: (1) initial pH-rise period, (2) the actual massive precipitation reaction starting at the maximal $\Omega_{calcite}$ value and (3) an equilibration phase. Calcium carbonate precipitation was evidenced by Ca concentration decrease and also supported by microscopic examination of produced mineral phases (see Section 3.4 below). Typical plots of bacterial biomass, pH, [Ca], [Alkalinity] and $\Omega_{calcite}$ as a function of elapsed time in biotic experiments in nutrient solution with and without light are presented Fig. 4. It can be seen from this figure that a significant decrease of calcium concentration is observed in both types of biotic experiments. This decrease is much more significant over the first five days of reaction under light compared with the darkness, although the initial calcite saturation index was similar in both experiments ($\Omega_{calcite} = 23$). Light experiments resulted in a significant increase of bacterial biomass, which was accompanied by a dramatic increase in solution pH, and as a result, $\Omega_{calcite}$ increase to 62, which coincided with the beginning of massive

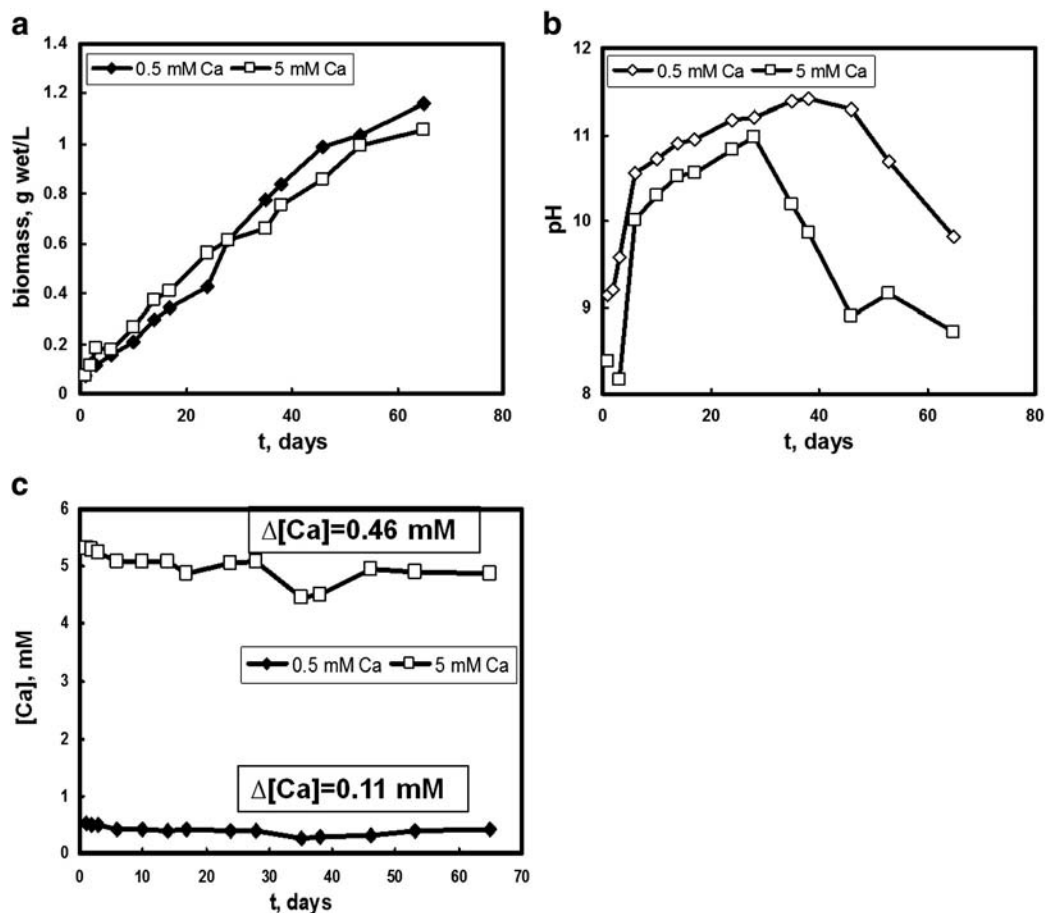


Fig. 3. Evolution of biomass (a), pH (b) and calcium concentration (c) in experiments with live *Gloeocapsa* sp. without mineral precipitation at different initial Ca concentration (Exp. 48, 51). The error bars are within the symbol size and represent the average of two duplicates.

calcium carbonate precipitation. In the absence of light, there were no increases of the biomass and pH. The Ω values remained stable or decreased by a factor of 1.5 to 3. These results suggest that the presence of active *Gloeocapsa* sp. crucially affect calcite precipitation rates compared with biotic controls without light. This corroborates the results of Obst et al. (2009b) who reported a factor of 1.4 to 1.5 increase in calcite precipitation rate in the presence of *Synechococcus leopoliensis* cyanobacteria under light compared with that under darkness, for Ω_{calcite} ranging from 6 to 8. Martinez et al. (2010) also observed the enhancement of CaCO_3 precipitation rate in biotic experiments with two strains of cyanobacteria *Synechococcus* sp. and *Planktothrix* sp. compared with bacteria-free experiments.

Biotic precipitation experiments were conducted at different initial Ω_{calcite} (from 1.5 to 150). The Ω_{calcite} evolution with time exhibited similar pattern among different experiments (see Fig. 5b and ESM). At the beginning of experiments, we observed an increase of Ω_{calcite} until a maximal value is attained, which induced massive CaCO_3 precipitation and subsequent Ω_{calcite} decrease. The duration of this increase and the maximal value of Ω_{calcite} varied from one experiment to the other depending on the initial experimental conditions (Fig. 5).

In contrast to biotic nutrient-rich experiments, in biotic experiments performed in the inert electrolyte solution, the Ca concentration decrease was much less pronounced (Fig. 6). During these experiments, only an insignificant increase of the biomass (between 0.3 and 0.08 $\text{g}_{\text{wet}} \text{L}^{-1}$) occurred, indicating the lack of bacterial development in the absence of nutrients (Fig. 6a). Despite the lack of bacterial growth, there was a significant pH increase in all biotic experiments performed in the inert electrolyte solution (from 8.9 at the beginning to 10.7 at the

end of experiment, Fig. 6b). The increase of pH without active development of bacterial biomass in the experiment in inert electrolyte solution may stem from on-going photosynthetic bacterial activity because of sufficient intracellular nutrient resources. As a result, calcite supersaturation degree increased from 66 to 90 at the beginning to 110–120 at the end of experiments with a maximum of ~190 attained at the first day of reaction. Despite such a significant supersaturation degree, very little CaCO_3 precipitation was observed in the inert electrolyte solution in the presence of live cells.

The main difference between experiments with live and inactivated cells is that pH and supersaturation degree rise in biotic experiments during photosynthesis whereas in experiments without bacteria or with dead cells, pH remains constant or decreases due to CaCO_3 precipitation. In this regard, abiotic experiments are considered as control runs. For this reason, they were performed in a limited number and the interpretation of calcification rates in these experiments is not statistically reliable.

Apparent precipitation rates (R) were calculated from the first derivative of the fluid phase Ca concentration with respect to time, using

$$R = \frac{\Delta[\text{Ca}]}{\Delta t} \quad (2)$$

This equation has been applied to each experimental data series, typically at stage 2 (Fig. 4), when the largest change in Ca concentration occurred. The resulting precipitation rates are listed in Table 2. The biomass-normalized rates of CaCO_3 precipitation in the nutrient

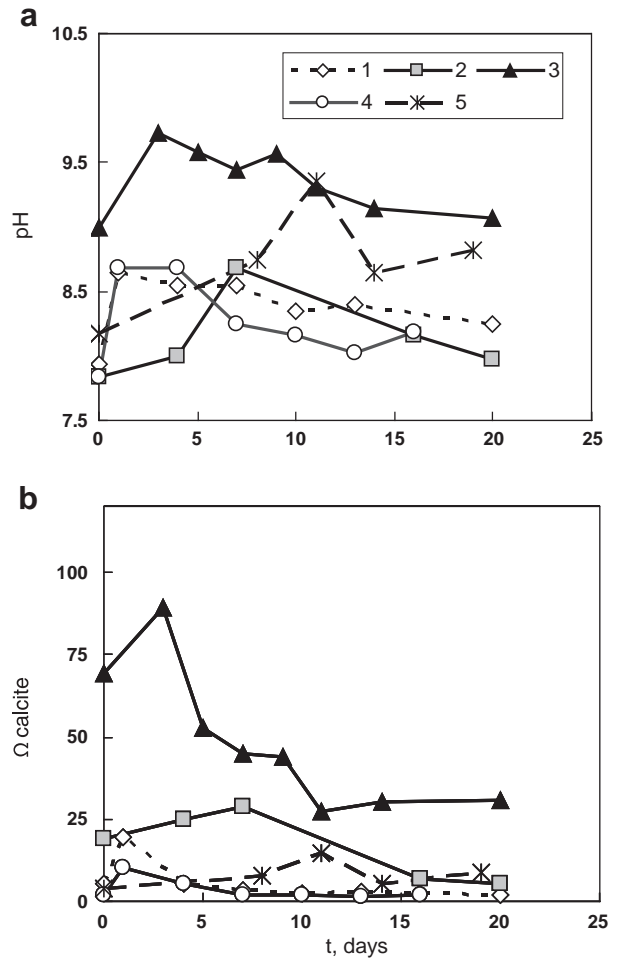
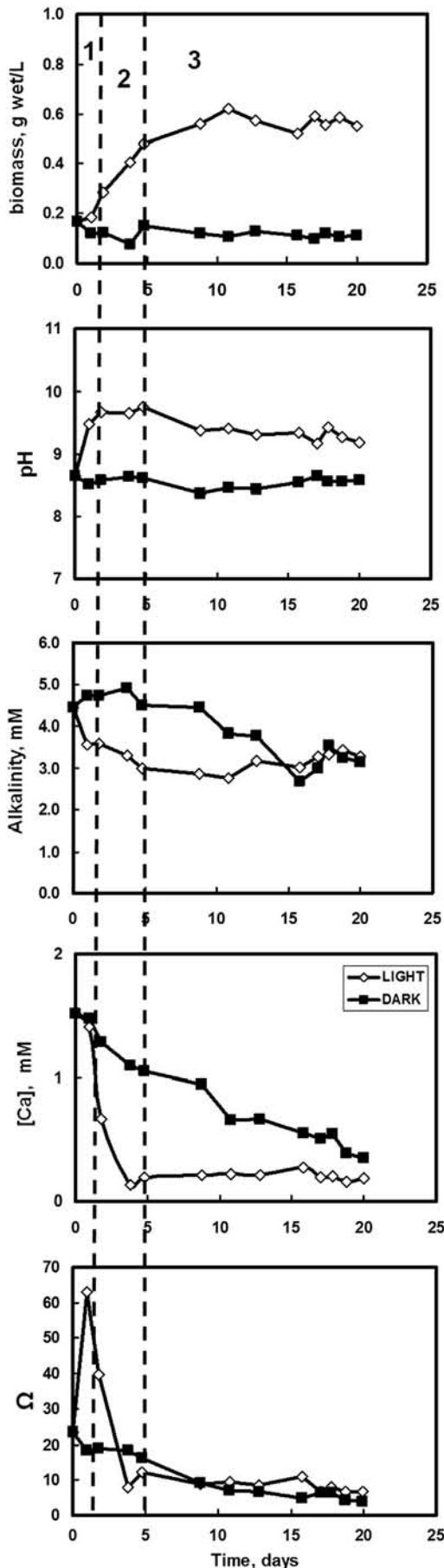


Fig. 5. Evolution of pH (a) and Ω_{calcite} (b) in biotic experiments in nutrient solution. The numbers in the legend correspond to the following initial experimental conditions: (1) 2 mM CaCl_2 , 4 mM NaHCO_3 , biomass 0.26 g_{wet}/L (Exp. 5); (2) 1 mM CaCl_2 , 8 mM NaHCO_3 , biomass 0.53 g_{wet}/L (Exp. 11); (3) 6 mM CaCl_2 , 2.5 mM NaHCO_3 , biomass 0.68 g_{wet}/L (Exp. 22); (4) 2 mM CaCl_2 , 1.6 mM NaHCO_3 , biomass 0.24 g_{wet}/L (Exp. 2); (5) 2.7 mM CaCl_2 , 1 mM NaHCO_3 , biomass 1.21 g_{wet}/L (Exp. 3).

solution range between 5 and 100 $\mu\text{mol h}^{-1} \text{g}_{\text{wet}}^{-1}$ with an average value of 36 $\mu\text{mol h}^{-1} \text{g}_{\text{wet}}^{-1}$ or 0.86 $\text{mmol d}^{-1} \text{g}_{\text{wet}}^{-1}$.

3.4. SEM and EDX characterization of precipitated mineral aggregates

In the course of experiments, visible white precipitates formed on the glass walls of the reactors and in the bacterial suspension after 5–7 days of culture growth. Whereas calcium carbonate precipitation was observed in all biotic experiments at $\Omega_{\text{calcite}} \geq 1.5$, calcium carbonate formation could be detected in abiotic experiments only at an initial $\Omega_{\text{calcite}} \geq 25$. The shape and size of precipitates in biotic and abiotic experiments were different. The SEM images of calcite formed in abiotic nutrient-free, biotic nutrient-free and biotic nutrient-rich solutions are shown in Figs. 7, 8 and 9, respectively. The XRD analysis identified solely calcite formation in all experiments except experiment 15 (Table 2) in nutrient media with an initial biomass 0.15 g_{wet} L⁻¹ at Ω_{calcite} of 30 that also produced aragonite. Abiotic nutrient-free experiments produced typical rhombohedral calcite crystals, 5 to 10 μm in size, often associated in

Fig. 4. Three phases of calcium carbonate precipitation by *Gloeocapsa* sp. in nutrient solution under light (open symbols) and in the darkness (solid symbols) (Exp. 12 and 38, respectively): (1) a pH-drift period, (2) massive precipitation, and (3) an equilibration phase.

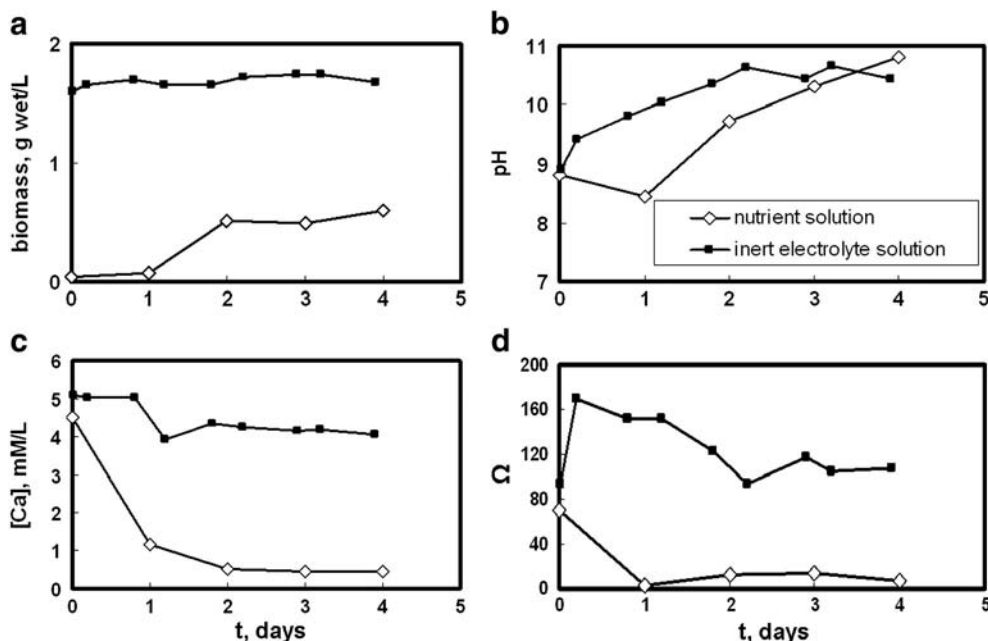


Fig. 6. Evolution of aqueous solution parameters during biotic experiments in nutrient solution and inert electrolyte solution (Exp. 24 and 37, respectively). Initial conditions: 5 mM CaCl_2 and 5 mM NaHCO_3 . (a) biomass evolution; (b) pH; (c) calcium concentration; (d) Ω_{calcite} .

clusters (Fig. 7). The size and shape of the crystals formed in biotic precipitation in the inert electrolyte and in the nutrient solution are drastically different and vary both in the course of the same experiment and among different initial solution conditions. First, there are large, 50 to 100 μm crystal associates without clear geometric form (Figs. 8a and 9c) or having spherical, rounded shapes of 5 to 15 μm in diameter (Fig. 8b). In both associated crystals, rounded and elliptical voids, 2 to 5 μm in diameter, most likely representing the imprints of *Gloeocapsa* sp. bacteria, are visible at the surface (Figs. 8c, d and 9a). The same imprints are also visible at the surface of crystals formed in nutrient-rich media (see below). Similar “porous” crystals have also been observed in experiments with CaCO_3 precipitation by algae (Stabel, 1986), cyanobacteria *Synechococcus*, eukaryotic picoplankton *Mychonastes* sp. and *Chlorella* sp. (Dittrich et al., 2004). The second possible type of precipitate is represented by rhomboid crystals with a longest facet of 10–15 μm (Fig. 8e), similar to those formed in abiotic experiments. The rhombohedral crystals and “porous” associates were often linked together, both in nutrient-free and nutrient-rich solutions (Figs. 8d and 9b). In addition, the rhombohedral and spherical associates of 10–15 μm in diameter were often formed in experiments with live cells in the inert electrolyte solution (Fig. 8f).

The third type of formed crystals is nano-globular associates. They were often found in biotic experiments in nutrient solution and represented by small individual crystals associated in large aggregates

(Fig. 9c), typically covered by organic matter, most likely in the form of exopolymeric substances (crystal-embedding veil distinguishable in Fig. 9d). The presence of organic matter is hypothesized based on results of the EDX analysis, which demonstrated very high C content at the surface of these crystals, much higher than that of the other surrounded crystals and on the difference of SEM images of the same areas taken in secondary and backscattered electrons modes.

The existence of different types of crystals in biotic experiments suggests that CaCO_3 precipitation is driven by different pathways: inorganic precipitation as indicated by the presence of rhombohedral crystals, typical for abiotic experiments and biologically affected precipitation indicated by the presence of the *Gloeocapsa*-size pores on the surfaces of crystals and the nano-globules covered by the organic matter.

3.5. CLSM, Raman and TEM characterization of Ca carbonate precipitation during *Gloeocapsa* photosynthesis

Concomitant CLSM and Raman micro-spectroscopy were used to detect and characterize the calcium carbonate associated to live bacterial cells in the course of the experiments. Systematic CLSM imaging of the bacterial suspensions from precipitation experiments during the first two weeks demonstrated that numerous cyanobacterial mucilage envelopes are covered by and sometimes completely encrusted in the

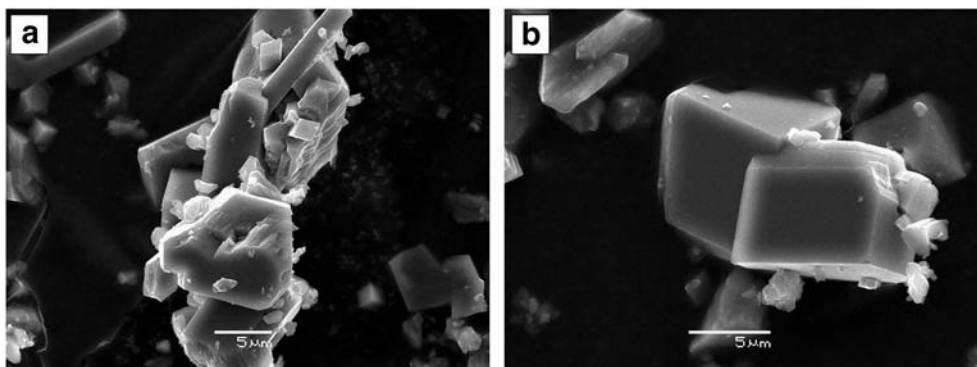


Fig. 7. SEM images of calcite precipitated in abiotic (cell-free BG 11) experiment (initial conditions: 20 mM CaCl_2 , 10 mM NaHCO_3) (Exp. 43).

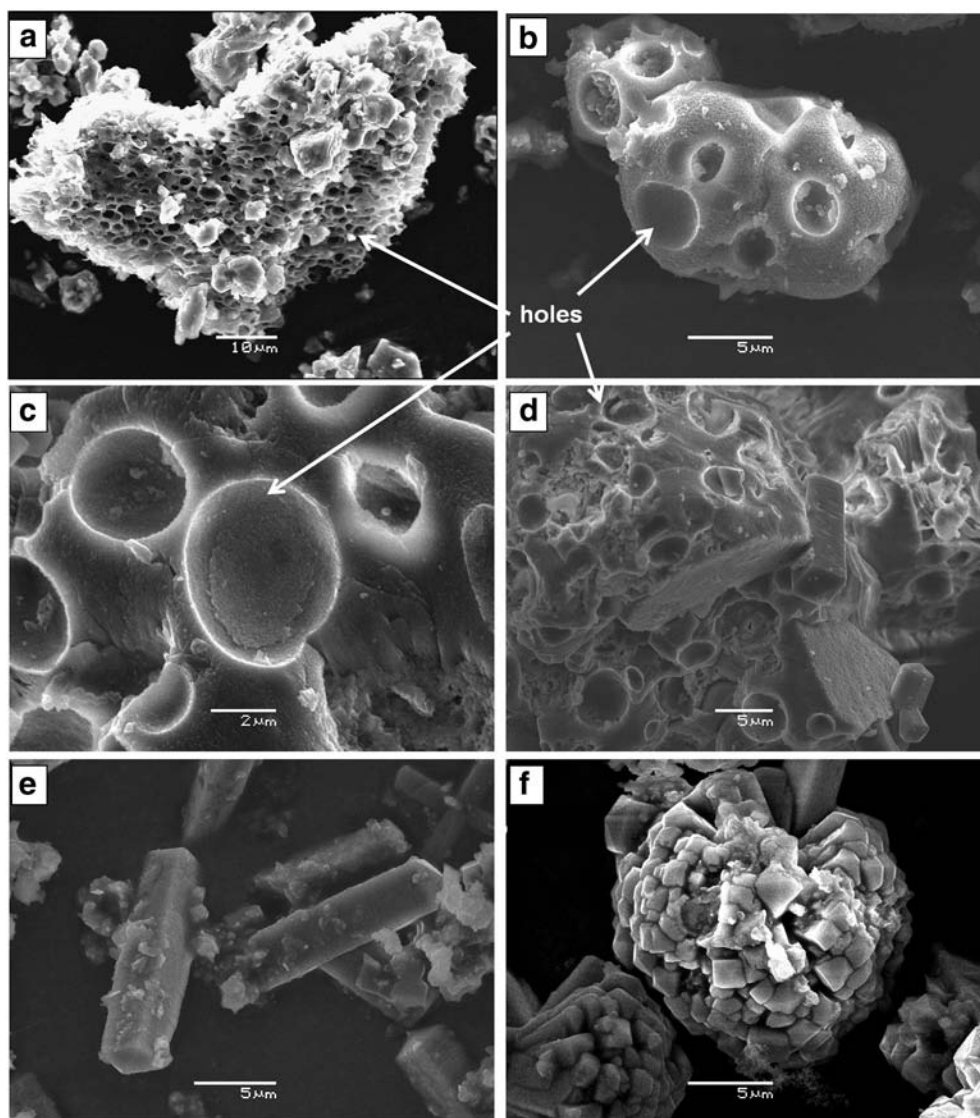


Fig. 8. SEM images of calcite formed in biotic experiments with *Gloeocapsa* sp. in inert electrolyte solution. (a, b) Exp. 34; (c, d) Exp. 37; (e, f) Exp. 36.

mineral represented by the green fluorescent agglomerates in the form of nanoglobules adjacent to the cells' mucilage envelopes or present outside the thick mucilage cell envelopes displaying a dark violet fluorescence (Fig. 10a, b). Some individual green spots at the surface of the mucilage envelopes provide evidence for carbonate nucleation at the cell surface. The associated Raman spectra of the mineral grains yielded the presence of calcite (Fig. 10c). As shown in Fig. 10(a, b), mineral precipitation is mainly associated with active bacteria displaying a red fluorescence and bacterial EPS. The size of these crystals is 200–500 nm.

Similar results were acquired using TEM on whole single cells and their surroundings. Representative examples of cells in the control (nutrient-rich, not supersaturated) and precipitation experiment (nutrient-rich, calcite-supersaturated) are shown in Fig. 11. The cells in the nutrient media appear intact without any traces of solid precipitates in the vicinity of the cells (Fig. 11a). The elements detected on and around live cells in nutrient medium are mainly C and O with minor S, Si, P, Cl and Na. No Ca was detected on cell surfaces. In contrast, significant CaCO_3 precipitation occurs in the vicinity of bacterial cells in calcite-supersaturated medium at $\Omega_{\text{calcite}} = 8$ to 24 (Fig. 11b). In these experiments, Ca was detected in precipitates formed at the surface and at some distances from *Gloeocapsa* sp. cells. The spatial organization

of these precipitates with respect to cyanobacterial cells is quite similar to that observed using CLSM (compare Figs. 11b and 10a–b). These comparable results are important because one of the major possible artifacts of TEM preparation as used in this work is the drying of bacteria–mineral associates which may lead to collapse of the precipitate on the cell wall, giving an impression of encrustation, while originally, the precipitation is more diffuse in the surrounding EPS. However, very similar features, including both tight attachment to the cell wall and diffuse aggregates of globules far from the cells, were detected both by TEM and CLSM. Therefore, we expect rather minor generation of artifacts using the TEM sample preparation technique adopted in this study.

The TEM images of cyanobacterial cells with mineral globules and agglomerates formed in the precipitation experiment are presented in Fig. 12. The size distribution of the globules is irregular; a large number of globules are in the 60–100 nm size range. These small globules are often attached to the surface of bacterial cells (Fig. 12a). Some cells may be completely covered by the globules so that the surface is not visible (Fig. 12b). A fraction of the encrusted cells could not be quantified solely from TEM images. There are also large globules (100–200 nm) that occur in the extracellular space, being separated from the *Gloeocapsa* sp. cells (Fig. 12c, d). Overall, comparison of Raman spectroscopy and CLSM imaging with TEM results demonstrate similar

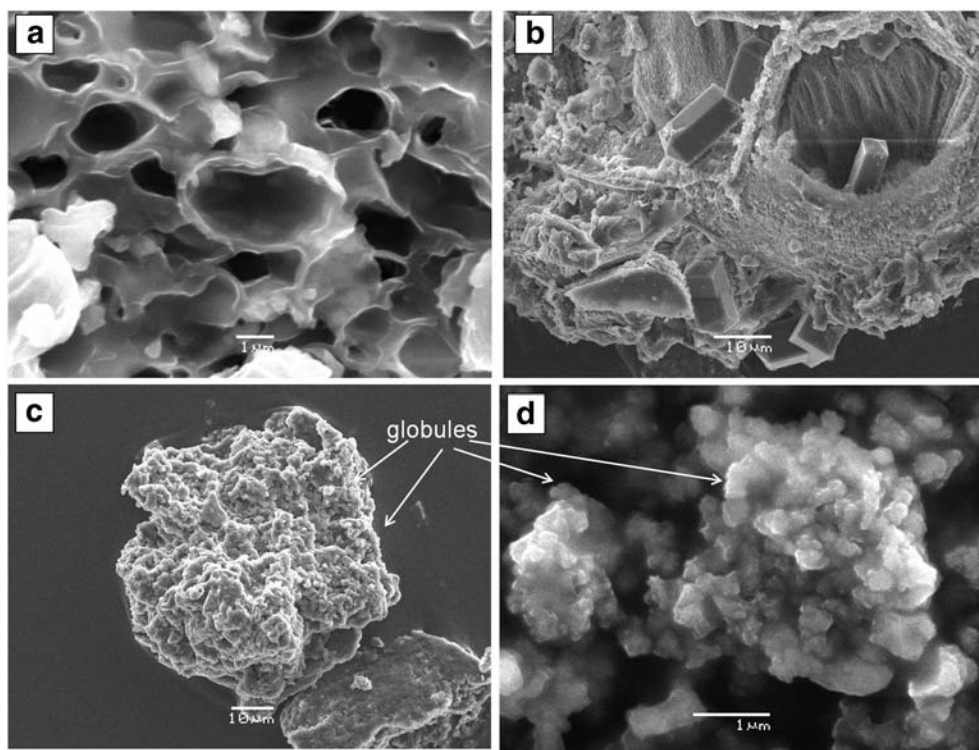


Fig. 9. SEM images of calcite precipitated in biotic experiment with *Gloeocapsa* sp. in nutrient solution (a) Exp. 31; (b, d) Exp. 14; (c) Exp. 12.

biocalcification pattern in terms of shape, composition and spatial organization of calcium carbonate (presumably calcite, see Fig. 10) nano- and microcrystals and active bacteria cells.

4. Discussion

4.1. Rates and mechanisms of calcium carbonate formation by *Gloeocapsa* sp.

The typical decrease of Ca concentration at the stage of massive CaCO_3 precipitation is 1 to 4 mM over the first 2 to 10 days, accompanied by a biomass increase of 0.2 to 0.5 $\text{g}_{\text{wet}}\text{L}^{-1}$ (Figs. 4, 6). This decrease, linked mainly to CaCO_3 precipitation ranges from 2 to 9 $\text{mmol g}_{\text{wet}}^{-1}$ over the first 10 days (Section 3.3) which is at least an order of magnitude higher than that induced by Ca adsorption at the cell surface (0.002 to 0.003 $\text{mmol Ca g}_{\text{wet}}^{-1}$, Section 3.1) and intracellular assimilation during cyanobacterial growth (0.086 to 0.43 $\text{mmol Ca g}_{\text{wet}}^{-1}$, Section 3.2). As a result, the rate of removal of Ca from the system during cyanobacterial cells growth is largely due to extracellular CaCO_3 precipitation rather than intracellular uptake and surface adsorption. It is noteworthy that the measured apparent bulk rates of CaCO_3 precipitation linked to *Gloeocapsa* sp. photosynthesis (5–80 $\mu\text{M h}^{-1}$, see Table 2) are similar or higher than those reported for the capsule-free cyanobacteria *Synechococcus* sp. and *Planktothrix* sp. (30–40 $\mu\text{M h}^{-1}$, Martinez et al., 2010), aerobic ureolithic bacteria (10 $\mu\text{M h}^{-1}$, Mitchell and Ferris, 2005) and anoxygenic phototrophic bacteria (5–130 $\mu\text{M h}^{-1}$, Bundeleva et al., 2012). At the same time, Lee et al. (2006) reported much lower Ca concentration decrease rate in the presence of *Synechococcus* sp. strain in 0.5 to 2.5 mM NaHCO_3 solution (2 to 8 $\mu\text{M h}^{-1}$). Note however, that *Gloeocapsa* cells used in our experiments were previously grown in the batch culture, so the cells were not at the same growth stage as those used by Lee et al. (2006). This difference could be responsible for different rates of calcium carbonate precipitation reported in different studies.

The results of the present work allowed establishment of a direct relationship between the amount of precipitated calcium and the amount of biomass produced during culture growth, as illustrated in Fig. 13

$$\Delta\text{Ca}_{\text{precipitated}}(\text{mmol}) = (2.0 \pm 0.2) \times \Delta\text{Biomass}_{\text{produced}}(\text{g}_{\text{wet}}) \quad (3)$$

Converting this relationship into molar scale and taking into account that the ratio of wet to dry biomass of *Gloeocapsa* is 10 ± 2 and that the proportion of carbon in dry biomass is 50% yields the molar inorganic Ca to organic C ratio in the reaction product of 0.48 ± 0.12 . This value is two-fold smaller than the theoretical $\text{Ca}/\text{C}_{\text{org}}$ ratio corresponding to CaCO_3 precipitation due to photosynthesis if the reaction is written in terms of the dominant C species in a neutral to alkaline pH range:



Several factors may be responsible for the smaller amount of sequestered CaCO_3 compared with the reaction stoichiometry, such as i) inhibition of calcite nucleation by the cell exometabolites allowing the solution to maintain elevated supersaturation degree, ii) decreased heterogeneous crystallization rate on already-formed nuclei because of surface passivation by dissolved organic matter and EPS and iii) enhanced production of extracellular polymeric substances by bacteria that lead to increases in organic matter yield without massive CaCO_3 precipitation.

Despite this clear tendency of active cells to precipitate CaCO_3 , there is no straightforward and statistically significant relationship between apparent calcite precipitation rates and maximal solution supersaturation degree before the onset of crystallization as illustrated in Fig. 14. The normalization of the apparent rates to the biomass present in the reactor or produced during the period of maximal [Ca] decrease did not improve the link between two parameters (Fig. 15). Note that experiments with *Synechococcus* and *Synechocystis* strains also demonstrated that the cell density does not have a direct effect on calcification rate (Lee et al.,

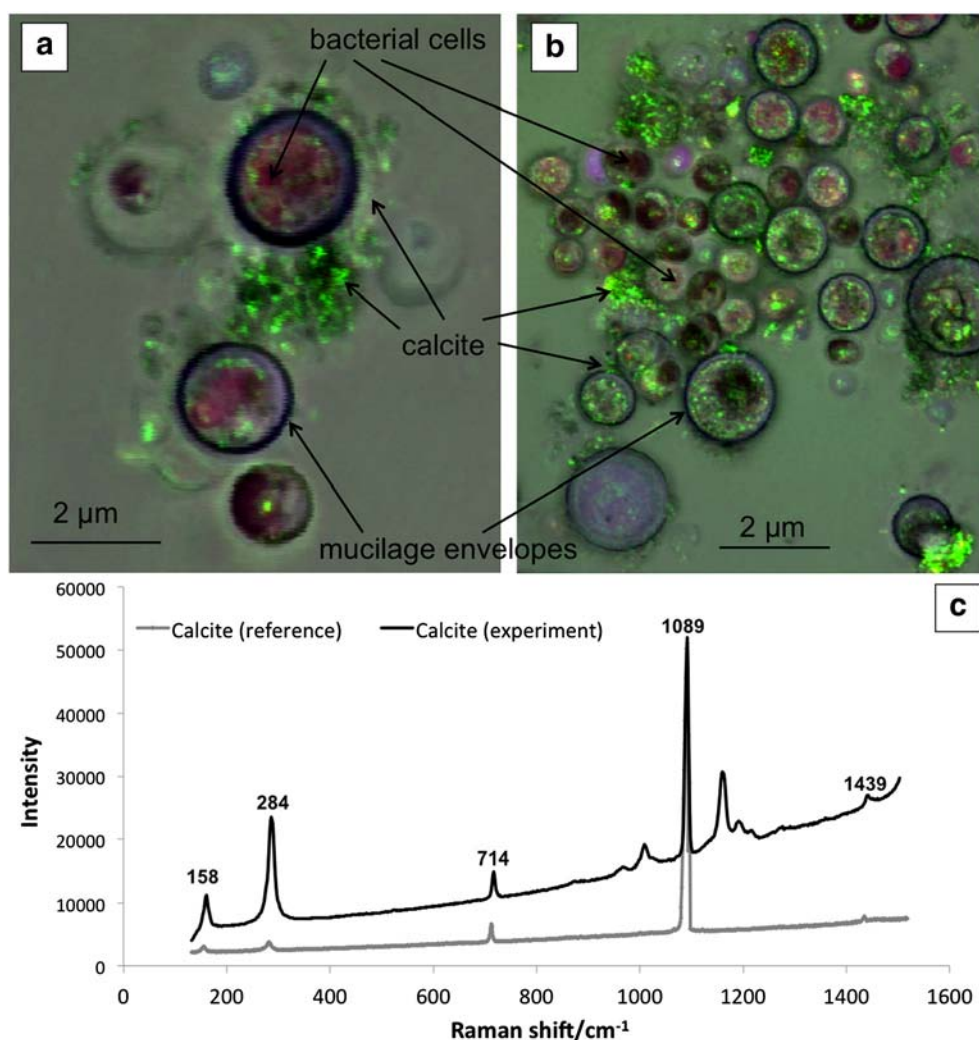


Fig. 10. Composite CLSM image of *Gloeocapsa* sp. cells (pigments of active bacterial cells and mucilage envelopes fluoresce in red and dark-violet colors, respectively) and globules of growing calcium carbonate (fluoresce in green) formed in Exp. 5, 7 (a and b, respectively). The fluorescence images superimposed on optical views in Differential Interference Contrast were obtained with a sequential excitation at 405, 515 and 633 nm, and fluorescence emission collected in the ranges 425–475, 520–550 and 640–800 nm. (c) Characteristic Raman spectrum of precipitated calcite collected following a laser irradiation of 785 nm. (For interpretation of the references to color in this figure legend, the reader is referred to the web version of this article.)

2004). No statistically significant correlations between biomass-normalized apparent precipitation rates R and the other parameters of aqueous solution (pH, Ca and DIC concentrations) were found. This indicates that the rate of carbonate precipitation in the presence of live cyanobacteria depends on both biotic and abiotic factors, including cell growth status and the rate of heterogeneous nucleation. The high scatter of experimental rates above an Ω_{calcite} of 50 in this study is certainly due to homogenous nucleation of CaCO_3 in strongly supersaturated solution and CaCO_3 heterogeneous nucleation onto bacterial cells acting as seeds. Significant variations in rates at low and moderate supersaturations may be due to 1) variations in the microenvironment of solution pH and supersaturation degree in the boundary layer adjacent to active photosynthesizing cells as it is known for natural settings (i.e., Shiraiishi et al., 2008) and 2) processes of Oswald ripening consisting of initial nucleation of amorphous CaCO_3 or monohydrocalcite at high supersaturation degree in the vicinity of cell surface, at Ω_{calcite} values significantly higher than that of the bulk solution, followed by rapid recrystallization of metastable phases to vaterite, aragonite and, finally, calcite. A discussion of the Oswald ripening during Ca(Mg) carbonate nucleation from supersaturated solution can be found in Pokrovsky (1998) and also has been demonstrated in experiments with anoxygenic phototrophic bacteria (Bundeleva et al., 2012). During mineral transformation

process, supersaturation state with respect to precipitating phase changes continuously. The overall Ca removal from solution represents the sum of Ca sinks into various polymorphic phases whose precipitation rates vary significantly as a function of aqueous solution composition. This may produce significant scatter in biocalcification rate as a function of Ω_{calcite} . The existence of aragonite as a final precipitate in Exp. 15 (Table 2) conducted at initial $\Omega_{\text{calcite}} \sim 30$, indirectly indicates such transformation reactions. It is also known that precipitation of amorphous CaCO_3 can serve as a protection mechanism against uncontrolled precipitation of calcite at cyanobacterial surfaces (Obst et al., 2009a). Moreover, the formation of CaCO_3 depends on the surface organic functional group and/or Ca concentration in the solution (see Liang et al., 2013 for discussion). CaCO_3 precipitation is induced by cell surface functional groups and occurs mainly via heterogeneous nucleation/crystal growth control in low Ca-solution. In solutions of high Ca^{2+} concentration, CaCO_3 precipitation mainly occurs due to spontaneous nucleation of unstable precursors followed by recrystallization towards more stable phases. Hence, biologically-induced carbonate mineral formation is a complex process whose kinetics can be controlled by numerous parameters (e.g. cell surface area, pH, Ca and DIC concentrations, supersaturation degree, surface functional group). As a result, although the overwhelming majority of removed Ca is due to

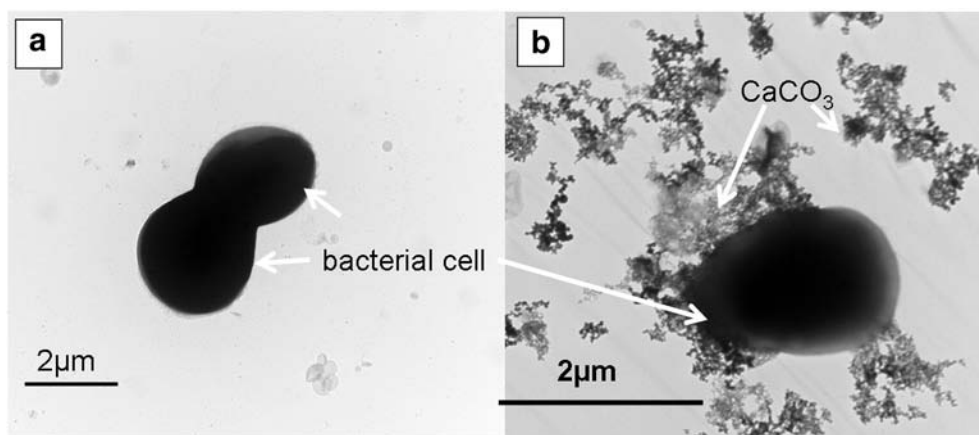


Fig. 11. TEM images of cells of *Gloeocapsa* sp. (a) in nutrient solution; (b) in calcite-supersaturated media (1 mM CaCl_2 , 10 mM NaHCO_3) (Exp. 14). CaCO_3 precipitated in the vicinity of the cell surface and at some distance.

photosynthesis-induced CaCO_3 formation, we cannot quantitatively distinguish between CaCO_3 formed in the vicinity of cells (microniches) and that massively precipitated in the bulk of supersaturated aqueous solution.

CaCO_3 precipitation by cyanobacteria *Gloeocapsa* sp. includes several consecutive stages. In the first step, the metal ions present in the aqueous surroundings of the cell interact electrostatically with negatively charged groups of cell surface and capsules (i.e., Douglas and Beveridge, 1998) and cell exopolymeric substances that may act as nucleation sites capable of accumulating significant quantities of Ca^{2+} (Dittrich and Obst, 2004). Once Ca is bound, it attracts the carbonate ion, given that cyanobacterial metabolism increases the microenvironmental pH facilitating transformation of DIC into CO_3^{2-} . This mechanism is driven by HCO_3^- uptake into the cell and its conversion by carbonic anhydrase to CO_2 and OH^- (Miller and Colman, 1980). The CO_2 is incorporated into the cell biomass, whereas the OH^- ions are released into the cells' microenvironment (Miller et al., 1990) and concentrated around the cells, and as a result, around and within the capsules. Indeed, *Gloeocapsa* sp. grown under light is capable of increasing solution pH from 8.5–8.6 to 9.5–9.6 and decreasing Ca concentration within 48 h due to CaCO_3 precipitation (Fig. 4). This observation is further confirmed by the microscopic (CLSM and TEM analyses) and spectroscopic (Raman) results: CaCO_3 precipitation is observed around bacterial cells (Figs. 10a, b; 11b, 12a) with some cells and cell associates being completely encrusted by calcite (Fig. 8a, b and c). An additional mechanism of cyanobacterial biomineralization, suggested first by Douglas and Beveridge (1998), involves cyanobacteria continuously shedding off patches of mineralized EPS layers, which is rapidly replaced by new material. The quantitative contribution of this mechanism to biocalcification of *Gloeocapsa* sp. cannot be determined in this study; however, given that precipitated CaCO_3 is located not only adjacent to the cells but also at some micron-scale distance from the cells surface (Figs. 10a, b, 11b and 12a, c and d), such an exopolysaccharidic shed-off pathway is certainly plausible. Therefore it could be hypothesized that polysaccharides constituting the capsule play a role comparable to that of the bacterial EPS layer in terms of Ca adsorption and removal from solution.

It is noteworthy that the typical spatial organization of cyanobacterial carbonate precipitates presented as honeycomb, highly porous calcite crystal associates, inheriting the capsule associates of bacteria (Figs. 8a, 9a). The CLSM and TEM images of cell- CaCO_3 precipitates revealed the tight link between the cell surface and the nano-globules of precipitated CaCO_3 . Similar nano-spheres and globules have been found during calcium carbonate precipitation by different bacteria (Sprachta et al., 2001; Dupraz et al., 2004; Aloisi et al., 2006). In the latter study, calcium carbonate precipitation was observed on EPS and near the microbial cell wall in the form of nano-globules. Other recent studies with other types of anaerobic and aerobic heterotrophic bacteria (e.g., Altermann et al., 2006;

Bontognali et al., 2008; Spadafora et al., 2010) also confirmed the governing role of mineral nano-globules in microbially induced Ca and Mg carbonate formation. The presence of EPS such as alginate is also known to produce the agglomeration of vaterite globules, a precursor of calcite, and decrease their rate of crystallization from supersaturated solution (Olderoy et al., 2009). As such, the association of nano-globules around the photosynthesizing cells observed in this and other studies indirectly suggests the governing role of cell EPS and mucilage as site of massive CaCO_3 formation.

The major surface functional groups of *Gloeocapsa* sp. cells are carboxylate, amine, phosphoryl/phosphodiester and hydroxyl because of the presence of protein, lipid and carbohydrate components on the external envelopes of cells and cell associates such as capsules (Pokrovsky et al., 2008). The lack of cell protection mechanisms against Ca adsorption in alkaline solutions is confirmed by the similar degree of Ca adsorption both in pH-dependent adsorption edge experiments, when the adsorption slightly increased with pH at $\text{pH} > 7$ and displayed no effect of light on the adsorption yield (Fig. 1) and the “Langmuirian” isotherm when the Ca adsorbed concentration was rather similar in circumneutral and alkaline solution (Fig. 2).

In contrast to other cyanobacteria such as *Synechococcus* sp. and *Planktothrix* sp. (Martinez et al., 2010) and anoxygenic phototrophic bacteria (Bundeleva et al., 2011), the *Gloeocapsa* sp. cells do not increase their zeta-potential at $9 \leq \text{pH} \leq 11$ (Pokrovsky et al., 2008). This result, together with the massive cell encrustation by CaCO_3 and mineral formation in the vicinity of the cell walls, microscopically confirmed in the present study, suggest the absence of a specific “cell protection mechanism” against cell encrustation during the active phase of CaCO_3 nucleation.

4.2. Application for natural settings and paleoenvironments

It was earlier argued that the sole action of cyanobacteria, notably in the biomats, is insufficient to provide massive calcium carbonate deposition. Numerous field observation and modeling experiments (Krumbein et al., 1977; Chafetz and Buczynski, 1992) have demonstrated that precipitation of calcium carbonate occurs predominantly within the mats in the aphotic zone, in the deeper parts of the mats where the degradation of organic compounds by heterotrophic bacteria occurs. For example, calcium carbonate precipitation in microbialites of lagoonal settings built by different *Phormidium* species of cyanobacteria was observed mainly in the interior of the domes and clearly separated from the photosynthetically active surface layer (Gautret et al., 2006). On the other hand, it has been demonstrated that the carbonate mineral lithification process occurs by decomposition of an amorphous matrix of bacterial exopolymer (not sheath material) in the photic zone across the stromatolite surface (Reid et al., 2000; Dupraz et al., 2013; Vasconcelos et al., 2013). In the latter

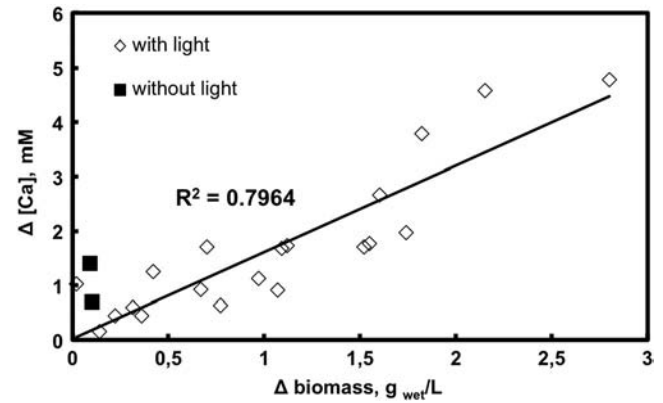
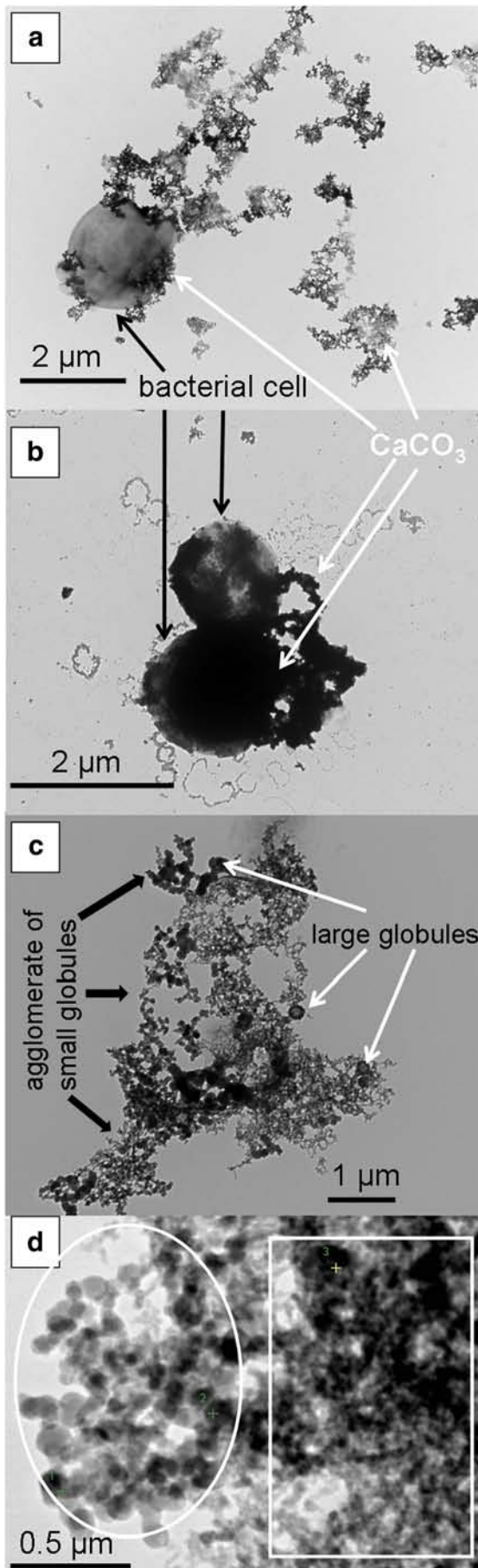


Fig. 13. Relationship between the amount of precipitated Ca (mM) and increase of the biomass (g_{wet}/L) in biotic experiments with *Gloeocapsa* sp. in nutrient solution. Experimental conditions: $\Omega_{\text{initial}} = 1.5\text{--}150$; pH = 7.8–9.6.

case, the action of heterotrophic bacteria in organic matter degradation is the main limiting step in carbonate mineral deposits.

In modern Ca–Mg carbonate stromatolites, which are formed in association with microbial mats in hypersaline coastal lagoons, the degradation of organic matter of soft mats leads to the development of lithified Ca–Mg carbonate laminate *via* sub-micron polyhedral crystal formation of high-Mg calcite and/or Ca dolomite as a result of the coalescence of carbonate nano-globules around degraded organic matter nuclei (Spadafora et al., 2010). Furthermore, dead cyanobacteria are coated with calcium carbonate quicker and to a greater extent than live cyanobacteria (Chafetz and Buczynski, 1992), which is in agreement with the earlier observation that CaCO₃ precipitation within the mats is governed by the degradation of organic carbon compounds by bacteria (Krumbein et al., 1977). In addition to well-established S-layer shed off (Thompson et al., 1997), the lack of calcification of viable cells may be linked to metabolic maintenance of positive surface potential and self-protection of live cyanobacterial cells from the encrustation (Martinez et al., 2008, 2010). Another mechanism of bacteria self-protection against uncontrolled encrustation are the extracellular polymeric substances secreted by the microbial community as it is the case for *Desulfovibrio brasiliensis*, whose cells are predominantly located outside of the EPS aggregates where mineral growth takes place. As a result, they remain mobile and are rarely entombed within the mineral (Bontognali et al., 2008). Similarly, another sulfate reducing bacterium, *Desulfonatronum lacustre*, produces individual globules, 6–20 nm in diameter, that originate from the cell surface but calcify significantly only when released to the culture medium (Aloisi et al., 2006). The idea that the EPS of cyanobacteria serve as effective Ca²⁺-buffers, thus preventing seed crystal nucleation even in a highly supersaturated macroenvironment, has also been suggested from numerous field studies of biofilms in alkaline salt lakes (e.g., Arp et al., 1999a, b; Arp et al., 2010; Dittrich and Sibling, 2010; Rogerson et al., 2010; Dupraz et al., 2013).

The possible absence of self-protection mechanisms against CaCO₃ incrustation in *Gloeocapsa* sp. sheds new light on the mechanisms and capacities of this cyanobacterium to form carbonate mineral deposits. In particular, the role of capsular cyanobacteria in the Precambrian aquatic environments could be more important compared with unicellular or filamentous microorganisms. Indeed, it follows from the results of this study that precipitation of CaCO₃ occurs in the vicinity of live *Gloeocapsa*

Fig. 12. TEM image of *Gloeocapsa* sp. cells and globules of calcium carbonate formed in calcite-supersaturated media (1 mM CaCl₂, 10 mM NaHCO₃). (a) General view of the bacterial cells and CaCO₃ precipitated in the vicinity of the cell surface and at some distance; (b) Cell aggregate completely covered by small CaCO₃ globules; (c) Extracellular globular associates; (d) Detail of globular associates with aggregates of small globules (white rectangle) and large globules (white oval). Aggregate of small globules attached to the cell (not shown in this picture) (Exp. 14).

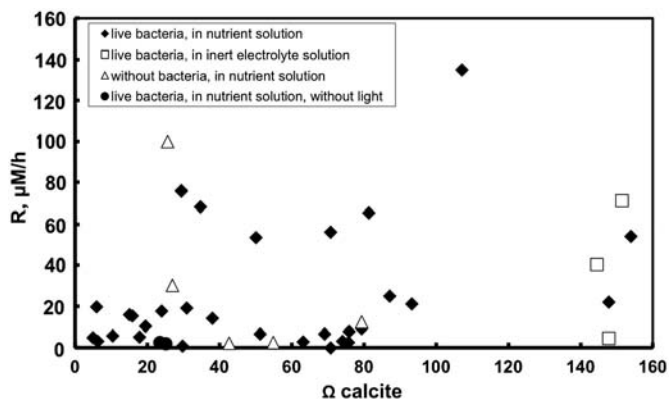


Fig. 14. Plot of apparent Ca precipitation rates ($\mu\text{M}/\text{h}$) as a function of calcite supersaturation degree in the bulk solution.

cells. As such, the increased pH rise adjacent to cells should promote *in vivo* cyanobacterial sheath calcification as it is expected for Proterozoic calcifying cyanobacteria (Riding, 2006). Similarly, cyanobacterial calcification in freshwater tufa stromatolites is mainly driven by the biofilm photosynthesis as indicated by microsensor data (Arp et al., 2010).

Although *Gloeocapsa* sp. cyanobacteria can be found in various natural settings from freshwater to hypersaline conditions, the application of the obtained results to marine environments, where microbial mat lithification results from complex interactions between various phototrophic and heterotrophic metabolism, both aerobic and anaerobic, is not straightforward. In these non-freshwater environments, the precipitation of CaCO_3 may be strongly inhibited by high concentration of Mg^{2+} (Riding, 1992) and within by a biofilm of dissolved, colloidal and particulate organic substances (Dupraz and Visscher, 2005). Moreover, most natural communities are partially composed of extracellular organic matter, displaying a large variety of states (from dissolved to gel), which is always the ultimate place where carbonate will nucleate regardless of the source of the supersaturation rise (photosynthesis or heterotrophic metabolism). An important result of the present study, most likely linked to the lack of self-protection mechanism, is the capacity of *Gloeocapsa* sp. to calcify without necessity of the destruction of EPS or cell death. Therefore, CaCO_3 production by these cyanobacteria in natural settings might not require the cells and their EPS being mineralized by heterotrophic bacteria, unlike for many other calcifying bacteria. This should allow *Gloeocapsa* sp. to efficiently calcify in the simplest ecological environment, even in monoculture. Moreover, in an alkaline Precambrian ocean, where large amounts of carbonate were formed, induction through sulfate reduction could be entirely ineffective (Meister, 2013), which refutes the previously claimed role of sulfate-reducing bacteria as the major players of massive CaCO_3 precipitation in these paleo-settings. In this regard, the action of

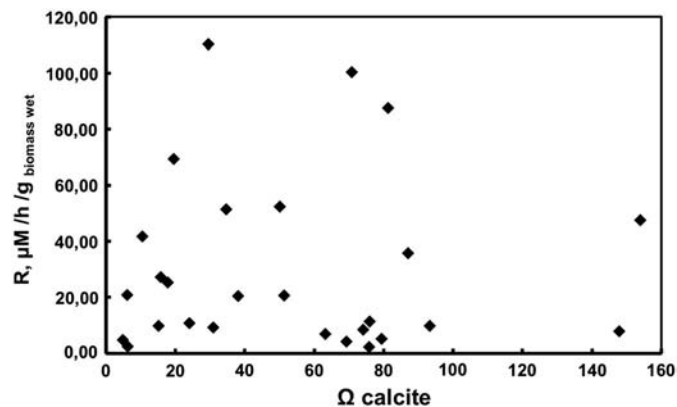


Fig. 15. Plot of apparent Ca precipitation rates ($\mu\text{M}/\text{h}/\text{g}_{\text{biomass wet}}$) in nutrient bulk solution as a function of calcite supersaturation degree.

cyanobacteria becomes most likely the sole driving force for local supersaturation rise and carbonate precipitation. As demonstrated in this experimental study, cyanobacteria *Gloeocapsa* sp. have a high capacity to precipitate CaCO_3 in a large range of supersaturation (Ω_{calcite} 1.5–150). As such these bacteria might represent important calcifying organisms in the highly alkaline ancient oceans (before 1000 Ma) (Arp et al., 2001) and also in various contemporary aquatic environments.

5. Conclusions

This study presents the first step towards the quantification of CaCO_3 precipitation by photosynthesizing cyanobacterium, *Gloeocapsa* sp., having atypical cellular organization. Biotic experiments performed in supersaturated solutions (Ω_{calcite} from 1.5 to 150) yielded different types of crystals, reflecting that CaCO_3 precipitation in these experiments can be driven by different mechanisms: inorganic precipitation producing rhomboid calcite crystals, encountered in abiotic experiments and cell-induced precipitation producing the porous crystals with honeycomb-like structure bearing the imprints of *Gloeocapsa* sp. cell associates. Detailed CLSM and TEM analyses revealed the presence of nano-globules associated with organic matter in the vicinity of the cell surface but also at some micron-scale distance from the cells. Overall, the microscopic examination of reaction products obtained in various environmental conditions does not suggest the existence of any self-protection mechanism against uncontrolled CaCO_3 encrustation of live *Gloeocapsa* sp. cells, which is in contrast to that established earlier for other cyanobacteria, anoxygenic phototrophic bacteria and heterotrophic anaerobic bacteria. The lack of this self-protection mechanism, also supported by electrostatic surface properties of *Gloeocapsa* sp. cell capsular associates, Ca adsorption on live and inactivated cells and high laboratory calcification rates as measured at relatively low biomass produced during bacterial growth, place these bacteria among the most efficient bacterial calcifiers on Earth. They are capable of calcifying in monoculture without heterotrophic bacterial component. The absence of a direct correlation between the apparent CaCO_3 precipitation rates and calcite supersaturation degree or other solution chemical composition parameters is most likely linked to specific microenvironments, non-detectable in the bulk solution, adjacent to cyanobacterial cell because of intensive photosynthetic activity and OH^- ion release.

Acknowledgments

This work was supported by the GRASP project (MRTNCT-2006-035868), INSU program “INTERVIE”, LIA “LEAGE” and BIO-GEO-CLIM Grant No. 14.B25.31.0001 of the Ministry of Education and Science of the Russian Federation. We are grateful to two anonymous reviewers for their constructive comments.

Appendix A. Supplementary data

Supplementary data to this article can be found online at <http://dx.doi.org/10.1016/j.chemgeo.2014.03.007>.

References

- Allison, J.D., Brown, D.S., Novo-Gradac, K.J., 1990. MINTEQA2/PRODEFA2—A Geochemical Assessment Model for Environmental Systems—Version 3.0 User's Manual: Environmental Research Laboratory, Office of Research and Development, U.S. Environmental Protection Agency, Athens, Georgia (106 pp.).
- Aloisi, G., Gloter, A., Kruger, M., Wallman, K., Guyot, F., Zuddas, P., 2006. Nucleation of calcium carbonate on bacterial nanoglobules. *Geology* 34, 1017–1020.
- Altermann, W., Kazmierczak, J., Oren, A., Wright, D.T., 2006. Cyanobacterial calcification and its rock-building potential during 3.5 billion years of Earth history. *Geobiology* 4, 147–166.
- Arp, G., Reimer, A., Reitner, J., 1999a. Calcification in cyanobacterial biofilms of alkaline salt lakes. *Eur. J. Phycol.* 34, 393–403.
- Arp, G., Thiel, V., Reimer, A., Michaelis, W., Reitner, J., 1999b. Biofilm exopolymers control microbialite formation at thermal springs discharging into the alkaline Pyramid Lake, Nevada, USA. *Sediment. Geol.* 126, 159–176.

- Arp, G., Reimer, A., Reitner, J., 2001. Photosynthesis-induced biofilm calcification and calcium concentrations in Phanerozoic oceans. *Science* 292 (5522), 1701–1704.
- Arp, G., Bissett, A., Brinkmann, N., Cousin, S., De Beer, D., Friedl, T., Mohr, K.I., Neu, T.R., Reimer, A., Shiraishi, F., Stackebrandt, E., Zippel, B., Reimer, A., 2010. Tufo-forming biofilms of German karstwater streams: microorganisms, exopolymers, hydrochemistry and calcification. *Geol. Soc. Lond., Spec. Publ.* 336, 83–118.
- Bazant, M.Z., Kilic, M.S., Storey, B.D., Aidari, A., 2009. Towards an understanding of induced-charge electrokinetics at large applied voltages in concentrated solutions. *Adv. Colloid Interf. Sci.* 152, 48–88.
- Bissett, A., Reimer, A., de Beer, D., Shiraishi, F., Arp, G., 2008. Metabolic microenvironmental control by photosynthetic biofilms under changing macroenvironmental temperature and pH conditions. *Appl. Environ. Microbiol.* 74 (20), 6306–6312.
- Bontognali, T.R.R., Vasconcelos, C., Warthmann, R.J., Dupraz, C., Bernasconi, S.M., McKenzie, J.T., 2008. Microbes produce nanobacteria-like structures, avoiding cell entombment. *Geology* 36, 663–666.
- Braissant, O., Decho, A.W., Dupraz, C., Glunk, C., Przekop, K.M., Visscher, P.T., 2007. Exopolymeric substances of sulfate-reducing bacteria: Interactions with calcium at alkaline pH and implication for formation of carbonate minerals. *Geobiology* 5, 401–411.
- Bundeleva, I.A., Shirokova, L.S., Bénéthet, P., Pokrovsky, O.S., Kompantseva, E.I., Balor, S., 2011. Zeta potential of anoxygenic phototrophic bacteria and Ca adsorption at the cell surface: possible implications for cell protection from CaCO₃ precipitation in alkaline solutions. *J. Colloid Interface Sci.* 360, 100–109.
- Bundeleva, I.A., Shirokova, L.S., Bénéthet, P., Pokrovsky, O.S., Kompantseva, E.I., Balor, S., 2012. Calcium carbonate precipitation by anoxygenic phototrophic bacteria. *Chem. Geol.* 291, 116–131.
- Bundeleva, I.A., Ménez, B., Augé, T., Bodéan, F., Recham, N., Guyot, F., 2014. Effect of cyanobacteria *Synechococcus* PCC 7942 on carbonation kinetics of olivine at 20 °C. *Miner. Eng.* 2–11.
- Castanier, S., Métauer-Levrel, G.L., Perthuisot, J.P., 1999. Ca-carbonates precipitation and limestone genesis—the microbiogeologist point of view. *Sediment. Geol.* 126, 9–23.
- Chafetz, H.S., Buczynski, C., 1992. Bacterially induced lithification of microbial mats. *Palaios* 7, 277–293.
- Couradeau, E., Benzerara, K., Gérard, E., Moreira, D., Bernard, S., Brown, G.E., Lopez-Garcia, P., 2012. An early-branching microbialite cyanobacterium forms intracellular carbonates. *Science* 336, 459462.
- Dittrich, M., Obst, M., 2004. Are picoplankton responsible for calcite precipitation in lakes? *Ambio* 33, 559–564.
- Dittrich, M., Sibler, S., 2005. Cell surface groups of two picocyanobacteria strains studied by zeta potential investigations, potentiometric titration, and infrared spectroscopy. *J. Colloid Interface Sci.* 286, 487–495.
- Dittrich, M., Sibler, S., 2006. Influence of H⁺ and calcium ions on surface functional groups of *Synechococcus* PCC 7942 cells. *Langmuir* 22, 5435–5442.
- Dittrich, M., Sibler, S., 2010. Calcium carbonate precipitation by cyanobacterial polysaccharides. *Geol. Soc. Lond., Spec. Publ.* 336, 51–63.
- Dittrich, M., Kurz, P., Wehrli, B., 2004. The role of autotrophic Picocyanobacteria in calcite precipitation in an oligotrophic lake. *Geomicrobiol. J.* 21, 45–53.
- Douglas, S., Beveridge, T.J., 1998. Mineral formation by bacteria in natural microbial communities. *FEMS Microbiol. Ecol.* 26, 79–88.
- Downs, R.T., 2006. The RRUFF Project: an integrated study of the chemistry, crystallography, Raman and infrared spectroscopy of minerals. Program and Abstracts of the 19th General Meeting of the International Mineralogical Association in Kobe, Japan (003–13).
- Dupraz, C., Visscher, P.T., 2005. Microbial lithification in marine stromatolites and hypersaline mats. *Trends Microbiol.* 13, 429–438.
- Dupraz, C., Visscher, P.T., Baumgartner, L.K., Reid, R.P., 2004. Microbe–mineral interactions: early CaCO₃ precipitation in a Recent hypersaline lake (Eleuthera Islands, Bahamas). *Sedimentology* 51, 745–765.
- Dupraz, C., Fowler, A., Tobias, C., Visscher, P.T., 2013. Stromatolitic knobs in Storr's Lake (San Salvador, Bahamas): a model system for formation and alteration of laminae. *Geobiology* 11, 527–548.
- Gallagher, K.L., Braissant, O., Kading, T.J., Dupraz, C., Visscher, P.T., 2013. Phosphate-related artifacts in carbonate mineralization experiments. *J. Sediment. Res.* 83 (1), 37–49.
- Gautret, P., De Wit, R., Camoin, G., Golubic, S., 2006. Are environmental conditions recorded by the organic matrices associated with precipitated calcium carbonate in cyanobacterial microbialites? *Geobiology* 4, 93–107.
- Gérard, E., Ménez, B., Couradeau, E., Moreira, D., Benzerara, K., Tavera, R., Lopez-Garcia, P., 2013. Specific carbonate–microbe interactions in the modern microbialites of Lake Alchichica (Mexico). *ISME J.* 1–13.
- Hunter, R.C., Phoenix, V.R., Saxena, A., Beveridge, T.J., 2010. Impact of growth environment and physiological state on metal immobilization by *Pseudomonas aeruginosa* PAO1. *Can. J. Microbiol.* 56, 527–538.
- Jiang, H.-B., Cheng, H.-M., Gao, K.-S., Qiu, B.-S., 2013. Inactivation of Ca²⁺/H⁺ exchanger in *Synechocystis* sp. strain PCC 6803 promotes cyanobacterial calcification by upregulating CO₂-concentrating mechanisms. *Appl. Environ. Microbiol.* 79, 4048–4055.
- Krumbein, W.E., Cohen, Y., Shilo, M., 1977. Solar Lake (Sinai). 4. Stromatolitic cyanobacterial mats. *Limnol. Oceanogr.* 22, 635–656.
- Lee, B.D., Apel, W.A., Walton, M.R., 2004. Screening of cyanobacterial species for calcification. *Biotechnol. Prog.* 20 (5), 1345–1351.
- Lee, B.D., Apel, W.A., Walton, M.R., 2006. Calcium carbonate formation by *Synechococcus* sp. strain PCC 8806 and *Synechococcus* sp. strain PCC 8807. *Bioresour. Technol.* 97, 2427–2434.
- Liang, A., Paulo, C., Zhu, Y., Dittrich, M., 2013. CaCO₃ biomineralization on cyanobacterial surfaces: insights from experiments with three *Synechococcus* strains. *Colloids Surf. B: Biointerfaces* 111, 600–608.
- Martinez, R.E., Pokrovsky, O.S., Schott, J., Oelkers, E.H., 2008. Surface charge and zeta potential of metabolically active and dead cyanobacteria. *J. Colloid Interface Sci.* 323, 317–325.
- Martinez, R.E., Gardés, E., Pokrovsky, O.S., Schott, J., Oelkers, E.H., 2010. Do photosynthetic bacteria have a protective mechanism against carbonate precipitation at their surfaces? *Geochim. Cosmochim. Acta* 74, 1329–1337.
- McConaughy, T., Whelan, J.F., 1997. Calcification generates protons for nutrient and bicarbonate uptake. *Earth Sci. Rev.* 42, 95–117.
- Meister, P., 2013. Two opposing effects of sulfate reduction on carbonate precipitation in normal marine, hypersaline, and alkaline environments. *Geology* 41 (4), 499–502.
- Merz, M.U.E., 1992. The biology of carbonate precipitation by cyanobacteria. *Facies* 26, 81–102.
- Merz, M.U.E., Schlue, W.R., Zankl, H., 1993. pH-Measurement in the sheath of calcifying filamentous cyanobacteria. *Biomineralization, Programs and Abstracts* 45, 48.
- Merz-Preiss, M., Riding, R., 1999. Cyanobacterial tufo calcification in tow freshwater streams: ambient environment, chemical thresholds and biological processes. *Sediment. Geol.* 126 (1–4), 103–124.
- Miller, A.G., Colman, B., 1980. Evidence for HCO₃⁻ transport by the blue-green alga (cyanobacterium) *Coccochloris penicostis*. *Plant Physiol.* 65, 397–402.
- Miller, A.G., Espie, G.S., Canvin, D.T., 1990. Physiological aspects of CO₂ and HCO₃⁻ transport by cyanobacteria. *Can. J. Bot.* 68, 1291–1302.
- Mitchell, A.C., Ferris, F.G., 2005. The coprecipitation of Sr into calcite precipitates induced by bacterial ureolysis in artificial groundwater: temperature and kinetic dependence. *Geochim. Cosmochim. Acta* 69, 4199–4210.
- Obst, M., Dynes, J.J., Lawrence, J.R., Swerhone, G.D.W., Benzerara, K., Karundakaran, C., Kaznatcheev, K., Tylliszczak, T., Hitchcock, A.P., 2009a. Precipitation of amorphous CaCO₃ (aragonite-like) by cyanobacteria: a STXM study of the influence of EPS on the nucleation process. *Geochim. Cosmochim. Acta* 73, 4180–4198.
- Obst, M., Wehrli, B., Dittrich, M., 2009b. CaCO₃ nucleation by cyanobacteria: laboratory evidence for a passive, surface-induced mechanism. *Geobiology* 7, 324–347.
- Obst, M., Wang, J., Hitchcock, A.P., 2009c. Soft X-ray spectro-tomography study of cyanobacterial biomineral nucleation. *Geobiology* 7, 577–591.
- Olderoy, M.O., Xie, M., Strand, B.L., Flaten, E.M., Sikorski, P., Andreassen, J.-P., 2009. Growth and nucleation of calcium carbonate vaterite crystals in presence of alginate. *Cryst. Growth Des.* 9 (12), 5176–5183.
- Parkhurst, D.L., Appelo, C.A.J., 1999. User's Guide to PHREEQC (Version 2)—A Computer Program for Speciation, Batch-Reaction, One-Dimensional Transport, and Inverse Geochemical Calculations. U. S. Geol. Surv. Water Resour. Investig. Rep. 99–4259, 310.
- Paulo, C., Dittrich, M., 2013a. 2D Raman spectroscopy study of dolomite and cyanobacterial extracellular polymeric substances from Khor Al-Adaid sabkha (Qatar).
- Paulo, C., Dittrich, M., 2013b. 2D Raman spectroscopy study of dolomite and cyanobacterial extracellular polymeric substances from Khor Al-Adaid sabkha (Qatar). *J. Raman Spectrosc.* 44, 1563–1569.
- Pokrovsky, O.S., 1998. Precipitation of aluminum and magnesium carbonates from homogeneous supersaturated solutions. *J. Cryst. Growth* 186, 233–239.
- Pokrovsky, O.S., Martinez, R.E., Golubev, S.V., Kompantseva, E.I., Shirokova, L.S., 2008. Adsorption of metals and protons on *Gloeocapsa* sp. cyanobacteria: a surface speciation approach. *Appl. Geochem.* 23, 2574–2588.
- Price, G.D., Maeda, S., Omata, T., Badger, M.R., 2002. Modes of active inorganic carbon uptake in the cyanobacterium, *Synechococcus* sp. PCC 7942. *Funct. Plant Biol.* 29 (2–3), 131–149.
- Rachel, R., Pum, D., Marda, J., Majs, D., Komrska, J., Krzyżanek, V., Rieger, G., Stetter, K.O., 1997. II. Fine structure of S-layers. *FEMS Microbiol. Rev.* 20, 13–23.
- Reid, R.P., Visscher, P.T., Decho, A.W., Stolz, J.F., Bebout, B.M., Dupraz, C., Macintyre, I.G., Paerl, H.W., Pinkney, J.L., Prufert-Bebout, L., Steppe, T.F., DesMarais, D.J., 2000. The role of microbes in accretion, lamination and early lithification of modern marine stromatolites. *Nature* 406, 989–992.
- Riding, R., 1992. Temporal variation in calcification in marine cyanobacteria. *J. Geol. Soc.* 149, 979–989.
- Riding, R., 2006. Cyanobacterial calcification, carbon dioxide concentrating mechanisms, and Proterozoic–Cambrian changes in atmospheric composition. *Geobiology* 4, 299–316.
- Rippka, R., Deruelles, J., Waterbury, J., Herdman, M., Stanier, R., 1979. Generic assignments, strain histories and properties of pure cultures of cyanobacteria. *J. Genet. Microbiol.* 111, 1–61.
- Rogerson, M., Pedley, H.M., Middleton, R., 2010. Microbial influence on macroenvironmental chemical conditions in alkaline (tufo) streams: perspectives from *in vitro* experiments. *Geol. Soc. Lond., Spec. Publ.* 336, 65–81.
- Sanchez-Roman, M., Vasconcelos, C., Schmid, T., Dittrich, M., McKenzie, J.A., Zenobi, R., Rivadeneyra, M.A., 2008. Aerobic microbial dolomite at the nanometer scale: Implications for the geologic record. *Geology* 36, 879–872.
- Shiraishi, F., 2012. Chemical conditions favoring photosynthesis-induced CaCO₃ precipitation and implications for microbial carbonate formation in the ancient ocean. *Geochim. Cosmochim. Acta* 77, 157–174.
- Shiraishi, F., Bissett, A., de Beer, D., Reimer, A., Arp, G., 2008. Photosynthesis, respiration and exopolymer calcium-binding in biofilm calcification (Westerhöfer and Deinschwanger Creek, Germany). *Geomicrobiol. J.* 25, 83–94.
- Spadafora, A., Perri, E., McKenzie, J.A., Vasconcelos, C., 2010. Microbial biomineralization processes forming modern Ca:Mg carbonate stromatolites. *Sedimentology* 57, 27–40.
- Sprachta, S., Camoin, G., Golubic, S., Le Campion, Th., 2001. Microbialites in a modern lagoonal environment: nature and distribution (Tikehau atoll, French Polynesia). *Palaeogeogr. Palaeoclimatol. Palaeoecol.* 175, 103–124.
- Stabel, H.H., 1986. Calcite precipitation in Lake Constance: chemical equilibrium, sedimentation, and nucleation by algae. *Limnol. Oceanogr.* 31, 1081–1093.

- [Thompson, J.B., Ferris, F.G., 1990. Cyanobacterial precipitation of gypsum, calcite, and magnesite from natural alkaline lake water. *Geology* 18, 995–998.](#)
- [Thompson, J.B., Shultze-Lam, S., Beveridge, T.J., Des Marais, D.J., 1997. Whiting events: biogenic origin due to the photosynthetic activity of cyanobacterial picoplankton. *Limnol. Oceanogr.* 42, 133–141.](#)
- [Vasconcelos, C., Dittrich, M., McKenzie, J., 2013. Evidence of microbiocoenosis in the formation of laminae in modern stromatolites. *Facies* 60, 1–11.](#)
- [Verrecchia, E.P., Freytet, P., Verrecchia, K.E., Dumont, J.L., 1995. Spherulites in calcrete laminar crusts: biogenic CaCO₃ precipitation as a major contributor to crust formation. *J. Sediment. Res.* 65, 690–700.](#)
- [Zinovieva, M., Fresneau, C., Arrio, B., 1998. Electrophoretic mobility variations of *Synechococcus* PCC 7942 plasmalemma vesicles with nitrogen source. *Bioelectrochem.* 46, 55–58.](#)